Response to Reviewers' Comments

We thank the editor and the anonymous reviewers for their helpful comments to improve our manuscript. A point-to-point response to reviewers' comments is provided below. We have also carefully revised the manuscript following the reviewers' recommendations. We hope that the revised manuscript meets the publication standards of *Atmospheric Chemistry & Physics*.

Reviewer #2

Major Comment:

I find this paper poorly referenced, and basically, this paper provides no new information except for the fact the measurements were made in China. As I suggested in my initial review this paper is not suitable for an international journal such as ACP.

Response: We respectfully disagree with the reviewer's assessment that this study provides no new information and is poorly referenced. There are multiple unique findings in the manuscript that provide new insights on land-atmosphere exchange of Hg. In particular, quantitative analysis of TGM evasion from five contrasting land covers in a forest catchment along with observations of TGM concentrations in soil pore gas with respect to soil depth was performed, which is rare in the literature. Detailed meteorological and environmental observations were made to support and interpret TGM emissions. The level of details in the field measurements make this work one of the more comprehensive study of TGM flux from soil. The observational data were applied to develop empirical models of TGM evasion in forest ecosystem with model parameters not previously considered in earlier studies. East Asia including China is the emission region that contributes to nearly 40% of global anthropogenic emissions of Hg. China has elevated level of atmospheric Hg concentration and deposition, and as a result high concentrations of Hg in surface soils. These conditions make the region important for characterizing air-soil exchange of Hg.

In the current study, long-term (130 days) and multi-plot (five plots) observations of soil-air fluxes coupled with soil pore Hg^0 were investigated to improve understanding on Hg evasion from soil in a subtropical forest. With simultaneous measurements of soil-air Hg fluxes and soil pore Hg^0 concentrations, the Hg^0 diffusion coefficients between soil and atmosphere were estimated, this fundamental information will be important for future modeling studies. Several aspects in this work demonstrate the novelty. First, long-term observations reduce the uncertainty and bias of temporal patterns of soil-air Hg fluxes. Second,

multi-plot observations reduce the uncertainty and bias of spatial patterns of soil-air Hg fluxes. Together, this detail improves overall ecosystem estimates of soil Hg evasion compared to previous studies.

Comment #1:

Line 63 please add Engle et al 1 regarding atmospheric ozone

Response: The reference has been added in line 63.

Comment #2:

Please remove the sentence that starts line 84 "This study is, to our knowledge." Do you have a research hypothesis that guided your work?

Response: The sentence has been deleted. We have clarified the hypothesis in the revised text "We hypothesize that the 130-day and multi-plot study of soil-air fluxes and the vertical soil distribution of TGM can reduce the uncertainty of temporal patterns and spatial analysis of soil-air Hg fluxes, and improve overall understanding and estimates soil evasion from forest ecosystems." line 98-101.

Comment #3:

Line that starts 106 this is simply not true. Please do a full literature search.

Response: The sentence has been deleted.

Comment #4:

Sentence line 160 –soil-air flux is also driven by processes occurring at the surface.

Response: The sentence has been revised and we deleted the phrase "underneath the soil surface layer".

Comment #5:

Again the authors need to do a more complete literature search. A couple of examples include 2-5

It is not as simple as Fick's law.

Response: We have reviewed the suggested literature and have provided the model details based on Zhang et al. (Atmospheric Environment 2002, 36, (5), 835-846.) in lines 207-221:

$$F = h_i \times (C_s - C_i) = h_s \times (C_s - C_a) = h_b \times (C_a - C_i) \quad (2)$$

where h_i (cm hr^{-1}) is the overall Hg exchange coefficient of soil-air exchange interface; h_s and h_b (cm hr^{-1}) are the mass transfer coefficients for the soil surface layer and the boundary layer, respectively; and C_s (ng m^{-3}) and C_a (ng m^{-3}) are the TGM concentrations in soil pore air and the soil surface atmosphere. Noting $C_s - C_i = (C_s - C_a) + (C_a - C_i)$ from Eq. (2), the two-resistance nature of the Hg soil-air exchange model is described as:

$$1/h_i = 1/h_s + 1/h_b \quad (3)$$

By Fick's law, h_s may be given by

$$h_s = D_s/Z \quad (4)$$

where D_s (m^2 hr^{-1}) is the molecular diffusion coefficient of Hg in soil and Z (m) is the thickness of the soil surface layer.

The diffusive vertical soil flux, (F, ng m^{-2} hr^{-1}) was calculated from the gradient of TGM concentration between soil air and the overlying atmosphere:

$$F = Ds \frac{C_S - C_a}{Z_j - Z_k} = Ds \frac{\Delta C}{\Delta Z} \quad (5)$$

where Z_j and Z_k are the soil layer depths."

Comment #6:

For your gold trap analyses how did you do this and what was your analytical precision?

Response: We have supplemented the discussion regarding Section 2.6 of the revised manuscript to describe the QA/QC used our experiments (lines 234-258):

"2.6. Quality Assurance and Quality Control (QA/QC)

Gold cartridges were used for sampling pore TGM simultaneously with TGM flux measurements over soil. All cartridges were transported to a laboratory at the TFP Forest Station for Hg determination using a cold vapor atomic fluorescence spectroscopy (CVAFS) detector (Brooks Rand III). The limit of detection, based on three times the standard deviation of replicate measurements of the blank was 1 pg. Based on the sampled air volume, the detection limits were <0.10 ng m^{-3}. The calibration curve was developed using Hg saturated air and had to have a correlation coefficient greater than 0.99 before the samples analysis could proceed. Before and after the measurement of the sampling cartridges in each day, standard Hg saturated air was injected to test the accuracy of the Hg analyzer. If the deviation of the measured Hg mass higher than 5%, new calibration curve would be developed.

A controlled volume of saturated Hg air at a known temperature was injected to measure Hg recovery from the gold cartridges before and after the campaigns in each season. The recoveries of gold cartridges before and after the operation ranged from 98.8 to 103.2% and 96.3 to 102.5% (show sample size and mean+-2.6%), respectively. The collection efficiency of Hg vapor by the gold cartridges was determined by connecting two cartridges in sequence and sampling the ambient air for 24 h in laboratory. For all cartridges, less than 1% Hg was detected on the second cartridges compared to the first cartridge, indicating that more than >99% of TGM was absorbed by the gold cartridges during the field operation. For comparison, Hg fluxes were measured by two chambers side by side simultaneously. Blanks of the soil TGM flux sampling systems were measured by placing the DFC on a quartz glass surface in the five plots. The sampling time for blank measurements was same as soil-air TGM flux measurements, which were collected at 8:00 and 17:00, representing night (17:00−8:00 of next day) and day (8:00−17:00) emissions, respectively. The averaged blank was 0.13 ± 0.21 ng m^{-2} h^{-1} (n=10), which was subtracted from the soil-air TGM flux for each season."

Comment #7:

For your flux chamber please provide dimensions' turnover rate etc. in the main text.

Response: We have moved the description of the DFC dimensions and turnover rate to the main text in the revised manuscript (lines 130-149):

"Semi-cylindrical quartz glass and open-bottom DFCs (4.71 L) were utilized during the sampling campaign. The area of the DFCs over the soil surface was 20 × 30 cm, with six inlet holes (1 cm diameter). At the outlet of the chamber, an orifice was connected to two exit tubes: one to a regulated suction pump with a flow rate of 10 L min^{-1} and the other to a gold cartridge for trapping outlet TGM. A sub-stream of air was trapped by a pair of gold quartz cartridges at a flow rate of 0.5 L min^{-1}, which was measured by an integrating volume flow meter. The chamber flushing flow turnover time (TOT) was 0.47 min. The soil Hg flux was calculated using the following equation:

$$F = (C_0 - C_i) \times Q/A \qquad (1)$$

where F is the soil Hg flux (ng m^{-2} hr^{-1}); C_o and C_i are the steady state Hg concentrations (ng m^{-3}) of the outlet and inlet air streams, respectively, which were calculated by the Hg mass detected in gold cartridges and the corresponding air volume; A is the surface area enclosed by the DFC; Q is the flow rate

of ambient air circulated through the DFC (10 L min^{-1})."

Comment #8:

For section 3.2 consider some references that provide the data and conclusions that are presented in Agan. Another reference to consider is 7. Pg 8 other references to consider include 8 and 2

Response: We have added 7 additional references (Carpi and Lindberg, 1998;Zhang et al., 2001;Howard and Edwards, 2018;Osterwalder et al., 2018;Ericksen et al., 2006;Gustin et al., 2002;Johnson et al., 2003) including the 3 references as the reviewer suggested.

Comment #9:

I do not understand how you made the soil gas contour points when you were only making measurements at one location.

Response: We are glad to clarify here. We measured the soil pore TGM at four locations and several soil depths for a period of 1 month in each season. This has been described in Section 2.4 of the original manuscript (lines 190-203):

"**2.4. Soil pore TGM measurement and diffusion coefficient**

The measurement of soil pore TGM was based on the method of Moore et al. (2011). Soil pore gas samples were sequentially collected from inverted Pyrex glass funnels installed at different soil horizons using a vacuum pump and Teflon tubing. The top diameter of the Pyrex glass funnel was 100 mm and the stem length was 100-mm. Hg in soil pore gas was collected on the gold quartz cartridges using a flow rate of 20 mL min^{-1}, which eliminated entrainment of ambient air and did not disturb the soil pore gas profile (Mason et al., 1994;Sigler and Lee, 2006). Flows for each funnel were controlled by a separate rotameter that was calibrated by mass flow rate meter at the beginning and end of each sampling period. In the spring, soil pore TGM was measured at plots A and D at depths of 3, 6 and 10 cm. In the subsequent summer, autumn and winter, soil pore TGM was measured at plots A, B, D and E at five depths, including the Oe-Oa soil horizon interface (3 cm depth), the Oa-A soil horizon interface (6 cm depth), 5 cm into the A soil horizon (10 cm depth), A2-B soil horizon interface (20 cm depth) and 5 cm into the C soil horizon (50 cm) in each plot. Saturated soil water precluded measurement of soil TGM at plot C (wetland) (Fig. 1)."

Comment #10:

Please check significant figures throughout the paper.

Response: We thank the reviewer for this suggestion. We have checked and make the numbers of significant figures consistent throughout the manuscript.

Comment #11:

Line 465 remember that just because there is a correlation it may not really mean anything.

Response: We have revised the sentence as (lines 554-560):

"Sigler and Lee (2006) showed that Hg emission originated from shallow (5 cm) depths in forest soils is mainly due to the production of soil pore TGM in the surface horizons. In our study, soil TGM fluxes were correlated [show statistics here!] with the gradient between soil pore concentrations at 2, 5 and 10 cm depths and the atmosphere (Fig. S10). TGM concentrations were highest at the surface depths and the values decreased with depth, suggesting that production and subsequent emission of Hg from soil is derived from the upper 10-cm depths."

Comment #12:

Line 483. I think photoreduction of Hg(II) deposited to the soil is an important process that needs to be considered and you need to rethink this. Doing a more complete literature search may help you quantify this process. Try also looking at Eckley 6, 9, 10

Response: We agree and have expanded this section of the manuscript to make sure that this point is clear (lines 567-577):

"However, in the open field, TGM diffusion coefficient was found to be up to 10 times higher in the daytime ($D_{s\ day}$: 0.099 $m^2\ hr^{-1}$) than for nighttime ($D_{s\ night}$: 0.0095 $m^2\ hr^{-1}$), with day and night ($D_{s\ day+night}$: 0.0408 $m^2\ hr^{-1}$). Note that, in the open field, the D*s* night was comparable to those in forest plots, but the D_s day was significantly higher. During daytime, especially in the open field, stronger solar radiation increased the reduction of Hg^{2+} on the soil surface and therefore resulted in a higher flux (higher D_s). Photo-reduction of Hg^{2+} in soil is important source of the Hg^0 emission, which may overestimate the diffusivity of TGM during daytime (Eckley et al., 2011a;Eckley et al., 2011b). Our results suggest that the formation of Hg^0 in the surface soil exposed to solar radiation likely led to an overestimation of D*s* in soil. Therefore, we assumed

that Ds night can be used represent the local diffusion coefficient (D*s*) (Fig. 6) and applied in future model development."

Reference:

1. Engle, M. A.; Sexauer Gustin, M.; Lindberg, S. E.; Gertler, A. W.; Ariya, P. A., The influence of ozone on atmospheric emissions of gaseous elemental mercury and reactive gaseous mercury from substrates. Atmospheric Environment 2005, 39, (39), 7506-7517.

2. Zhang, H.; Lindberg, S. E.; Marsik, F. J.; Keeler, G. J., Mercury Air/Surface Exchange Kinetics of Background Soils of the Tahquamenon River Watershed in the Michigan Upper Peninsula. Water, Air, & Soil Pollution 2001, 126, (1), 151-169.

3. Zhang, H.; Lindberg, S. E.; Barnett, M. O.; Vette, A. F.; Gustin, M. S., Dynamic flux chamber measurement of gaseous mercury emission fluxes over soils. Part 1: simulation of gaseous mercury emissions from soils using a two-resistance exchange interface model. Atmospheric Environment 2002, 36, (5), 835-846.

4. Zhang, H.; Lindberg, S.; Gustin, M.; Xu, X. H., Toward a better understanding of mercury emissions from soils. Biogeochemistry of Environmentally Important Trace Elements 2003, 835, 246- 261.

5. Briggs, C.; Gustin, M. S., Building upon the Conceptual Model for Soil Mercury Flux: Evidence of a Link Between Moisture Evaporation and Hg Evasion. Water Air and Soil Pollution 2013, 224, (10).

6. Eckley, C. S.; Gustin, M.; Miller, M. B.; Marsik, F., Nonpoint source Hg emissions from actice industrial gold mines-2. Influential variables and annual emission estimates. In University of Nevada-Reno: Reno, p 13.

7. Johnson, D. W.; Benesch, J. A.; Gustin, M. S.; Schorran, D. S.; Lindberg, S. E.; Coleman, J. S., Experimental evidence against diffusion control of Hg evasion from soils. Science of the Total Environment 2003, 304, (1-3), 175-184.

8. Carpi, A.; Lindberg, S. E., Application of a Teflon (TM) dynamic flux chamber for quantifying soil mercury flux: Tests and results over background soil. Atmospheric Environment 1998, 32, (5), 873-882.

9. Eckley, C. S.; Gustin, M.; Marsik, F.; Miller, M. B., Measurement of surface mercury fluxes at active industrial gold mines in Nevada (USA). In University of Nevada-Reno: Reno, p 19.

10. Eckley, C. S.; Gustin, M.; Miller, M. B.; Marsik, F., Nonpoint source Hg emissions from active industrial

gold mines-influential variables and annual emission estimates. In University of Nevada-Reno: Reno, p 14.

Soil emissions, soil air dynamics and model simulation of gaseous mercury in subtropical forest

Jun Zhou [a, b, c], Zhangwei Wang [a, b, *], Xiaoshan Zhang [a, b], Charles T. Driscoll [d], Che-Jen Lin [e]

a. Research Center for Eco-Environmental Sciences, Chinese Academy of Sciences, Beijing 100085, China.

b. University of Chinese Academy of Sciences, Beijing 100049, China.

c. Key Laboratory of Soil Environment and Pollution Remediation, Institute of Soil Science, Chinese Academy of Sciences, Nanjing 210008, China.

d. Department of Civil and Environmental Engineering, Syracuse University, 151 Link Hall, Syracuse, New York 13244, United States.

e. Center for Advances in Water and Air Quality, Lamar University, Beaumont, Texas 77710, United States.

* Corresponding author: Zhangwei Wang

E-mail address: wangzhw@rcees.ac.cn(Z. Wang); Phone: +86 10 62849168.

No.18 Shuangqing Road, Beijing 100085, China

First author e-mail: zhoujun@issas.ac.cn (J. Zhou); Phone: +86 25 86881319.

No.73 East Beijing Road, Nanjing 210008, China.

Abstract: Evasion from soil is the largest source of mercury (Hg) to the atmosphere in terrestrial ecosystems. To improve understanding of controls and reduce uncertainty in estimates of forest soil-atmosphere exchange, soil-air total gaseous Hg (TGM) fluxes and vertical profiles of soil pore TGM concentrations were measured simultaneously for 130 days. The soil-air TGM fluxes, measured using dynamic flux chambers (DFC), showed patterns of both emission and deposition at five study plots, with an area-weighted net emission rate of 3.2 ng m^{-2} hr^{-1}. The highest fluxes and net soil Hg emission were observed for an open field, with lesser emission rates in coniferous (pine) and broad-leaved (camphor) forests, and net deposition in a wetland. Fluxes showed strong positive relationships with solar radiation, soil temperature and soil Hg concentrations, and negative correlations with ambient-air TGM concentration and soil moisture. Using experimental field observations and quadratic relationships with the five parameters, four empirical models were developed to estimate soil-air TGM fluxes. The highest TGM concentrations in soil gas consistently occurred in the upper mineral horizons of the coniferous (pine) forest and in the organic horizon of the broad-leaved forest. Strong correlations between fluxes and TGM concentrations in upper soil horizons (0–10 cm) suggest that TGM in the pores of surface soil acts as the source for diffusion to the atmosphere. Diffusion coefficients (D_s) of TGM between soil and atmosphere were calculated for the field sites, with the range of 0.0042–0.013 m^2 hr^{-1}. These values should provide a foundation for future model development.

Keywords: soil-air flux; modeling; budget; soil profile of gaseous Hg; diffusion coefficient

1. Introduction

Global long-range atmospheric transport and deposition is the main pathway of mercury (Hg) input to remote ecosystems (Grigal, 2003;Obrist et al., 2018;Beckers and Rinklebe, 2017). Soils account for more than 90% of Hg stored in terrestrial ecosystems (Obrist, 2012;Zhou et al., 2017a). While most studies have focused on the Hg derived from anthropogenic emissions, recent global Hg models estimate that 3600 Mg yr^{-1} of atmospheric Hg is deposited to terrestrial surfaces, with 1000 Mg yr^{-1} re-emitted back to the atmosphere (Outridge et al., 2018). Additionally, compared to anthropogenic emissions of Hg (2500 Mg yr^{-1}), estimates of re-emissions from soil surfaces are highly uncertain (Agnan et al., 2016;Outridge et al., 2018;Wang et al., 2018). Compiling data from 132 studies, Agnan et al. (2016) found that the Earth's surface (particularly in East Asia) is an increasingly important source of total gaseous Hg (TGM) emissions, contributing up to half of the global emissions from natural sources. They estimated terrestrial TGM emissions of 607 Mg yr^{-1}, but with a large uncertainty range of −513 to 1353 Mg yr^{-1}.

Forest soil receives Hg input from: 1) throughfall that wash out deposited Hg(II) on foliage surface; 2) litterfall that contain foliage uptake of atmospheric Hg^0; and 3) direct dry deposition to soil from the atmosphere (Grigal, 2003;Teixeira et al., 2018;Risch et al., 2017). Mercury outputs from forests soil occur from surface or subsurface runoff and air-surface evasion. Forest soils are highly complex media, with important characteristics that affect air-soil exchange, including soil physio-chemical characteristics (e.g., porosity, oxygen availability, redox potential, organic matter, and pH) (Moore and Castro, 2012;Obrist et al., 2010). Other factors also influence this process, such as meteorological conditions (e.g., solar radiation, air temperature, precipitation) (Eckley et al., 2015;Li et al., 2010;Zhou et al., 2015), atmospheric chemistry (ozone, nitrate radicals) (Peleg et al., 2015;Engle et al., 2005), atmospheric TGM concentrations (Wang et al., 2007) and biological processes (Obrist et al., 2010;Chen et al., 2017). Therefore, to characterize and quantify land-atmosphere exchange of TGM and eventually model global terrestrial sources to the atmosphere, it is necessary to understand the roles of these factors in mediating this process.

Research should also be devoted to investigate the reduction of ionic Hg (Hg^{2+}) on soil surfaces, the release of Hg^0 into soil pore gas, and the transport of Hg^0 in soil pores to ambient air from soils to better understand the soil Hg^0 evasion processes (Sigler and Lee, 2006). Numerous studies have researched soil-air Hg exchange by direct observations in the field or controlled laboratory

experiments (Gustin et al., 1997;Carpi and Lindberg, 1998;Choi and Holsen, 2009;Briggs and Gustin, 2013;Eckley et al., 2015;Osterwalder et al., 2018). A few studies have directly measured pore Hg concentrations within intact soils in the field (Moore and Castro, 2012;Obrist et al., 2017;Obrist et al., 2014;Sigler and Lee, 2006) and the laboratory (Pannu et al., 2014) to characterize and quantify soil Hg^0 formation. To date, only two study has examined TGM concentrations in soil pores and soil-air flux simultaneously (Obrist et al., 2017;Sigler and Lee, 2006), while one was limited in temporal and spatial resolution (Sigler and Lee, 2006). The dynamics of gaseous Hg concentrations in soil profiles, the potential diffusive redistribution of pore Hg^0 in soils, and the contribution of surface soils to the supply of atmospheric Hg are poorly understood and limit the development of models of land-atmosphere exchange of TGM.

Field studies have shown that elevated anthropogenic Hg emissions in South-East Asia have resulted high atmospheric Hg deposition regionally (Kumari et al., 2015;Pan et al., 2010). Forests experience highly elevated Hg loads, especially in China (Fu et al., 2015;Wang et al., 2016). The annual loading of THg to subtropical forests in China have been shown to be much higher than some forest catchments in Europe and North America (Wright et al., 2016;Larssen et al., 2008). High Hg deposition has resulted elevated the soil Hg pools in Chinese subtropical forests (Wang et al., 2018;Wang et al., 2009;Zhou et al., 2013). Forest ecosystems not only act as Hg sinks, but can also serve as sources of previously deposited Hg. The forest area of China is 2.08×10^4 km^2, with more than half occurring as subtropical forest. Therefore, it seems likely that subtropical forest in China, which receives elevated atmospheric Hg deposition may also be an important atmospheric Hg source as previous deposited Hg is re-emitted back to the atmosphere.

In this paper, we present results of 130-day and multi-plot (five) study of soil-air fluxes and the vertical distribution in soil gas of TGM in a subtropical forest located in Tieshanping Forest Park (TFP) in China. The study was conducted over four seasons in 2014. The aims of this investigation were to (1) conduct field measurements to reduce the uncertainty in soil-air fluxes of TGM in forest catchments; (2) improve and parameterize an empirical model of soil Hg evasion over complex terrain; and (3) understand how vertical profiles of TGM in soil pores evolve temporally and spatially and are related to soil-air exchange of Hg. We hypothesize that the 130-day and multi-plot study of soil-air fluxes and the vertical soil distribution of TGM can reduce the uncertainty of temporal patterns and spatial analysis of soil-air Hg fluxes, and improve overall understanding and

101 estimates soil evasion from forest ecosystems.

102 **2. Materials and methods**

103 **2.1. Study area**

104 The flux measurements were conducted in a Masson pine (*Pinus massoniana* Lamb.) stand
105 (conifer), which was planted in 1960s following a complete destruction of a natural Masson pine
106 forest at Tieshanping Forest Park (TFP) (106°41.24′E, 29°37.42′N). The forest is located about 20
107 km northeast of Chongqing City, at an altitude from 200 to 550 m (Fig. S1). The mean annual
108 precipitation is 1028 mm, with 75% of the rainfall occurring from May to October. The mean annual
109 air temperature is 18.2 ℃. The total area of the study forest is 1.06×10^3 ha in the TFP (Fig. S1).

110 The stand is homogeneous, dominated by Masson pine, with some associated species,
111 including camphor (*Cinnamom camphora*) and Gugertree (*Schima superba* Gardn. et Champ). The
112 soil is typically mountain yellow earth (corresponding to an Acrisol in the FAO), with clay
113 mineralogy dominated by kaolinite (Zhou et al., 2018b). The pH and soil organic matter (SOM) of
114 the organic soil horizons (excluding undecomposed litter, about 4 cm) averaged at 3.8±0.16 and
115 13%±4.3%, respectively. The pH and SOM of upper mineral soil horizons (4 cm under the organic
116 horizons) averaged 3.9 ± 0.11 and 4.8% ± 1.0%, respectively (Zhou et al., 2015). Total Hg
117 concentrations in the organic soil horizons and mineral top horizons ranged from 54 to 462 ng g^{-1}
118 and from 23 to 160 ng g^{-1}, respectively (Zhou et al., 2015). Hg concentrations in environment media
119 are provided in the Supporting Information (SI, Supporting Text).

120

121 **2.2. Dynamic flux chamber (DFC) measurement**

122 To reduce the spatial uncertainty in Hg fluxes, different ecosystems were selected for study in
123 a sub-catchment in the TFP of Chongqing, including a coniferous forest (plots A and B), a wetland
124 (plot C), a broad-leaved (camphor) forest (plot D) and an open field with bare soil (plot E) (Fig. 1).
125 To reduce temporal uncertainty in Hg fluxes, 130-days of flux observations were undertaken over
126 four seasons (about one-month of continuous observations for each season) in 2014. Plot A was
127 positioned on the top of the hill slope; plot B was in the middle of the hill slope; plot C was in the
128 wetland within a coniferous forest; plot D was in broad-leaved (evergreen) forest and plot E is in
129 open field. Details of the plot instrumentation and sampling period are summarized in Table S1.

130 Semi-cylindrical quartz glass and open-bottom DFCs (4.71 L) were utilized during the

sampling campaign. The area of the DFCs over the soil surface was 20 × 30 cm, with six inlet holes (1 cm diameter). At the outlet of the chamber, an orifice was connected to two exit tubes: one to a regulated suction pump with a flow rate of 10 L min^{-1} and the other to a gold cartridge for trapping outlet TGM. A sub-stream of air was trapped by a pair of gold quartz cartridges at a flow rate of 0.5 L min^{-1}, which was measured by an integrating volume flow meter. The chamber flushing flow turnover time (TOT) was 0.47 min. The soil Hg flux was calculated using the following equation:

$$F = (C_0 - C_i) \times Q/A \qquad (1)$$

where F is the soil Hg flux (ng m^{-2} hr^{-1}); C_o and C_i are the steady state Hg concentrations (ng m^{-3}) of the outlet and inlet air streams, respectively, which were calculated by the Hg mass detected in gold cartridges and the corresponding air volume; A is the surface area enclosed by the DFC; Q is the flow rate of ambient air circulated through the DFC (10 L min^{-1}).

High flow rates and short TOT are appropriate for measuring flux from soils with high Hg concentrations, while lower flow rates and TOT are more appropriate for soils with low Hg concentrations. Eckley et al. (2010) suggested that the optimal flow was at the beginning of the stable $C_0 - C_i$ (ΔC) period, which was chosen as a compromise between competing criteria aimed at creating conditions inside the DFC similar to the adjacent outside air. Our previous study showed that when the ΔC was relative stable, the corresponding flushing flow rate was from 5 to 10 L min^{-1} (Zhou et al., 2017b). To void suppression the Hg emission potential due to the excessive buildup of Hg within the chamber, the flow rate of ambient air circulated through the DFC was 10 L min^{-1}.

The pair of gold cartridges were collected twice a day: every morning (about 8:00) and afternoon (about 17:00) representing night (17:00−8:00 of next day) and day (8:00−17:00) emissions, respectively. Twenty gold quartz cartridges were alternated during the sampling program. Additionally, diurnal variations of soil-air Hg fluxes were also conducted in each season, with gold cartridges collected every half an hour. A total of four diurnal measurements were conducted over the study, with diurnal variations were measured one day per season. It has been reported that the DFC method can introduce measurement bias under the given design flushing air flow rates and environmental condition (Lin et al., 2010;Zhang et al., 2002). The DFC enclosure imposes a physical constraint that can lead to accumulation to or evasion from the soil surface under measurement. Extensive examinations have been performed for selecting the experimental condition. We followed recommendations made by Eckley et al. (2010) for our measurements.

2.3. Empirical models of soil-air Hg fluxes

Models have been applied to estimate Hg emissions from soil to the atmosphere. Previous empirical models estimating soil Hg evasion have not considered the potential synergistic and antagonist relationships with environmental factors controlling land-atmosphere exchange. For this study, we extended the model developed from factorial simulation experiments by Lin et al. (2010) by modeling daily average Hg fluxes as a function of a number of environmental factors, including the effects of solar radiation, soil temperature, soil Hg concentrations, atmospheric Hg concentrations and soil moisture. Based on the measured TGM flux and a two-layer diffusion model (Zhang et al., 2002), ambient TGM concentrations should not be ignored when estimating TGM evasion in forest soils. Four predictive models were developed from multivariate regression analysis using the Hg fluxes measured by DFC for different ecosystems grouped into the four land-cover categories: coniferous forest, wetland, broad-leaved forest and open field. The Masson pine forest represents the coniferous forest, the camphor forest depicts the broad-leaved forest, the bare soil represents an open field, and the soil experiencing alternating dry-wet conditions represents a wetland. A model representing whole sub-catchment using the data from all the landscape plots was empirically developed separately.

For each plot, the datasets of fluxes measured by DFC and corresponding environmental factors (meteorological parameters and soil parameters) from four seasons were compiled. If the individual environmental factors and the interaction terms were determined to be significant, their effects were incorporated into a multivariate surface response analysis to understand the process variability. This approach allowed for weighing the effects of environmental conditions in the nonlinear regression analyses, which was used to develop the final predictive models of soil Hg flux. Data analyses (estimate of effects and ANOVA) of the factorial experiments were performed using Spss Statistics 17.0. Nonlinear regression analyses and their visualization were performed using MATLAB with the Statistics Toolbox. Predictive models were developed from daily flux observations with corresponding environmental factors for the four land-cover categories: coniferous forest (plot A), wetland (plot C), broad-leaved forest (plot D) and open field (plot E).

2.4. Soil pore TGM measurement and diffusion coefficient

The measurement of soil pore TGM was based on the method of Moore et al. (2011). Soil pore gas samples were sequentially collected from inverted Pyrex glass funnels installed at different soil horizons using a vacuum pump and Teflon tubing. The top diameter of the Pyrex glass funnel was 100 mm and the stem length was 100-mm. Hg in soil pore gas was collected on the gold quartz cartridges using a flow rate of 20 mL min^{-1}, which eliminated entrainment of ambient air and did not disturb the soil pore gas profile (Mason et al., 1994;Sigler and Lee, 2006). Flows for each funnel were controlled by a separate rotameter that was calibrated by mass flow rate meter at the beginning and end of each sampling period. In the spring, soil pore TGM was measured at plots A and D at depths of 3, 6 and 10 cm. In the subsequent summer, autumn and winter, soil pore TGM was measured at plots A, B, D and E at five depths, including the Oe-Oa soil horizon interface (3 cm depth), the Oa-A soil horizon interface (6 cm depth), 5 cm into the A soil horizon (10 cm depth), A2-B soil horizon interface (20 cm depth) and 5 cm into the C soil horizon (50 cm) in each plot. Saturated soil water precluded measurement of soil TGM at plot C (wetland) (Fig. 1).

Soil-air flux is the relationship of the dynamic diffusion between TGM concentrations in soil pores and TGM in the atmosphere, suggesting that soil Hg^0 formation and diffusion influence the soil-air flux. Based on the analogy of Ohm's law (Zhang et al., 2002):

$$F = h_i \times (C_s - C_i) = h_s \times (C_s - C_a) = h_b \times (C_a - C_i) \quad (2)$$

where h_i (cm hr^{-1}) is the overall Hg exchange coefficient at the soil-air interface; h_s and h_b (cm hr^{-1}) are the mass transfer coefficients for the soil surface layer and the boundary layer, respectively; and C_s (ng m^{-3}) and C_a (ng m^{-3}) are the TGM concentrations in soil pore air and the soil surface atmosphere. Noting $C_s - C_i = (C_s - C_a) + (C_a - C_i)$ from Eq. (2), the two-resistance nature of the Hg soil-air exchange model is described as:

$$1/h_i = 1/h_s + 1/h_b \quad (3)$$

By Fick's law, h_s may be given by

$$h_s = D_s/Z \quad (4)$$

where D_s (m^2 hr^{-1}) is the molecular diffusion coefficient of Hg in soil and Z (m) is the thickness of the soil surface layer.

The diffusive vertical soil flux, (F, ng m^{-2} hr^{-1}) was calculated from the gradient of TGM concentration between soil air and the overlying atmosphere:

$$F = Ds\ \frac{C_S - C_a}{Z_j - Z_k} = Ds\frac{\Delta C}{\Delta Z} \quad (5)$$

where Z_j and Z_k are the soil layer depths.

2.5. Environmental measurements.

At each sampling location, soil samples were collected from the DFC footprint (0−5 cm). Soil Hg and SOM concentrations were determined. Soil percent moisture and temperature were monitored with Time Domain Reflectometry (TDR) Hydra Probe II (SDI−12/RS485) and a Stevens water cable tester (USA). Solar radiation was measured by a weather station (Davis Wireless Vantage VUE 06250 Weather Station, Davis Instruments, Hayward, CA) located in the TFP Forest Station about 500 m away from the plots. The total Hg concentrations in soil samples were determined using a DMA-80 direct Hg analyzer (Milestone Ltd., Italy) and the SOM content in soils were determined using the sequential loss on ignition (LOI) method (Zhou et al., 2013). Detail of the measurements is summarized in the SI.

2.6. Quality assurance and quality control (QA/QC)

Gold cartridges were used for sampling pore TGM simultaneously with TGM flux measurements over soil. All cartridges were transported to a laboratory at the TFP Forest Station for Hg determination using a cold vapor atomic fluorescence spectroscopy (CVAFS) detector (Brooks Rand III). The limit of detection, based on three times the standard deviation of replicate measurements of the blank was 1 pg. Based on the sampled air volume, the detection limits were <0.10 ng m^{-3}. The calibration curve was developed using Hg saturated air and had to have a correlation coefficient greater than 0.99 before the samples analysis could proceed. Before and after the measurement of the sampling cartridges in each day, standard Hg saturated air was injected to test the accuracy of the Hg analyzer. If the deviation of the measured Hg mass higher than 5%, new calibration curve would be developed.

A controlled volume of saturated Hg air at a known temperature was injected to measure Hg recovery from the gold cartridges before and after the campaigns in each season. The recoveries of gold cartridges before and after the operation ranged from 98.8 to 103.2% and 96.3 to 102.5% (show sample size and mean+-2.6%), respectively. The collection efficiency of Hg vapor by the gold

cartridges was determined by connecting two cartridges in sequence and sampling the ambient air for 24 h in laboratory. For all cartridges, less than 1% Hg was detected on the second cartridges compared to the first cartridge, indicating that more than >99% of TGM was absorbed by the gold cartridges during the field operation. For comparison, Hg fluxes were measured by two chambers side by side simultaneously. Blanks of the soil TGM flux sampling systems were measured by placing the DFC on a quartz glass surface in the five plots. The sampling time for blank measurements was same as soil-air TGM flux measurements, which were collected at 8:00 and 17:00, representing night (17:00−8:00 of next day) and day (8:00−17:00) emissions, respectively. The averaged blank was 0.13 ± 0.21 ng m^{-2} h^{-1} (n=10), which was subtracted from the soil-air TGM flux for each season.

3. Results and discussion

3.1. Landscape- and forest species-dependence of soil-air hg fluxes at the forest catchment scale

The soil TGM flux measurements for the five plots were calculated for the day and night and reported as mean daily fluxes with standard deviations (SD) (Fig. 2). Over the course of the campaigns, net TGM emission was observed at the open field (24 ± 33 ng m^{-2} hr^{-1}), coniferous forest (upper elevation 3.5 ± 4.2 ng m^{-2} hr^{-1}, mid elevation 2.8 ± 3.9 ng m^{-2} hr^{-1}) and the broad-leaved forest (0.18 ± 4.3 ng m^{-2} hr^{-1}), while net deposition was evident at the wetland (−0.80 ± 5.1 ng m^{-2} hr^{-1}), respectively.

This pattern suggests that soil-air Hg fluxes at catchment scale vary by soil properties (e.g., soil Hg concentration, moisture, SOM) and forest species composition. High variability (SD and coefficient of variation (SD/mean, range of 119−2374%)) was evident in daily Hg fluxes largely driven by meteorological variation, demonstrating that measurements over several days may exhibit considerable temporal variability and long-term study should be undertaken to reduce the uncertainty in temporal patterns.

The mean TGM flux in the open field was about 8.6 times higher than that under the forest canopy ($p< 0.001$). Our results are consistent with Ma et al. (2013) and Xin and Gustin (2007), showing large Hg evasion following forest conversion to bare soils due to direct exposure to sunlight, as fluxes were enhanced by increases in solar radiation and temperature. Due to frequent heavy rains

in the catchment, a large amount of surface runoff impacted the wetland (plot C). Elevated runoff may have decreased Hg and SOM in surface soils due to erosion (Table 1). This site had the lowest Hg^0 fluxes of the plots studied (overall net sink). In addition, soils in the wetland plot were mostly saturated throughout the year, limiting Hg fluxes and likely contributing to the sink behavior. This pattern is consistent with previous studies by Kyllonen et al. (2012), Selvendiran et al. (2008) and Lindberg et al. (1998) that soil Hg evasion can be inhibited by wet conditions. However, our results are in contrast to the findings of earlier studies that showed soil wetness accelerates Hg^0 release from soil (Gustin, 2003;Kocman and Horvat, 2010) and increases in soil water often result in a decrease of soil redox potential (Zarate-Valdez et al., 2006) leading to enhanced reduction of Hg^{2+} to Hg^0. It is likely that the soil has been saturated with water such that Hg^0 evasion is inhibited (Briggs and Gustin, 2013;Gustin and Stamenkovic, 2005).

In the broad-leaved (camphor) forest (plot D), litterfall deposition was twice as high as that in the coniferous (pine) forest (plots A and B) (Zhou et al., 2018b), resulting in greater shielding of sunlight to the surface soil and limiting soil Hg evasion. Increases in sunlight can both increase solar radiation and soil temperature, which can enhance the photochemical reduction of Hg^{2+} on the soil surface and Hg^0 evasion after its formation from Hg^{2+}. Moreover, some studies have reported significantly higher Hg inputs with a larger fraction occurring as throughfall fluxes from conifers than hardwoods (Blackwell et al., 2014). Throughfall Hg is likely more reactive than litter Hg (Renner, 2002) and subsequently higher inputs and a higher throughfall fraction could contribute to higher Hg evasion from the coniferous (pine) forest. In the mid-slope of the pine stand (plot B), soil Hg concentration was elevated compared to the upslope plot (Table 1), corresponding with higher soil Hg fluxes. The forest canopy not only influences the soil Hg concentration by atmospheric Hg deposition, but also alters soil physio-chemical properties (e.g. SOM, pH, porosity) which affect soil-air exchange. For example, the annual litterfall Hg deposition flux at the broad-leaved forest (91 μg m^{-2} yr^{-1}) was approximately two times greater than the coniferous forest (41 μg m^{-2} yr^{-1}) (Zhou et al., 2018b); conversely, the SOM and soil Hg concentration in the broad-leaved forest were lower than the coniferous forest. Moreover, litter decomposition rate was lower, but the Hg mass accumulation in the litter was much higher in the coniferous forest compared to the broad-leaved forest (Zhou et al., 2018b), which resulted in seemingly inconsistent patterns between litterfall mass and SOM, as well as litterfall Hg deposition and soil Hg concentrations. Tree species can change soil physicochemical

properties (e.g. SOM, soil Hg concentrations), which influences soil-air exchange. These biological factors may have contributed to the much lower TGM evasion in the broad-leaved forest than the coniferous forest (Fig. 2).

Most studies measured soil TGM fluxes at only one location or at a single forest stand to characterize the whole ecosystem. Our observations clearly show that soil-air Hg fluxes vary substantially across different plots (Table 1), indicating that forest type/cover and landscape position significantly affect the TGM fluxes and therefore the flux variability among different sub-plots must be considered. Based on the areal distribution of each plot type (coniferous upland and mid-slope, broad-leaved, wetland, open) in the study sub-catchment (4.6 ha) (Table S1), the area-weighted TGM flux was 3.2 ng m^{-2} hr^{-1} for the entire catchment. The area-weighted TGM flux was 14% higher than plot A and 16% lower than plot B of the Masson pine stand. The observations from the campaigns at several plots with diverse forest cover in this study should reduce the overall uncertainty associated with soil-air fluxes of TGM in the overall forest catchment.

Soil TGM fluxes not only exhibited clear seasonal variations at all the plots, but also were responsive to seasonal and meteorological patterns. The fluxes were generally highest in the summer (Fig. 2), which showed net emissions at all the five plots, followed by spring, autumn, with the lowest values in the winter, which exhibited net deposition at all plots with the exception of plot B. The observed seasonal variation was dependent on sunlight because solar radiation drives photochemical reduction of Hg^{2+} (note the correlation between the TGM fluxes and solar radiation, Fig. S2). Additionally, greater solar radiation increases temperature, which promotes the production of soil Hg gas by biological and thermal processes (discussed in detail in the next section). We also observed strong variation in TGM evasion under different weather conditions. Rain events decreased TGM fluxes at all plots (Fig. S3) the rainwater reduced soil pore space and led to reduced evasion out of the soil. Therefore, the 130-day observations reduce the uncertainties and bias of temporal patterns of soil-air Hg fluxes and multi-plot observations reduce the uncertainties and bias associated with spatial analysis and improve overall ecosystem estimates soil evasion compared to previous studies, which confirms our hypothesis.

3.2. Correlations between environmental factors and fluxes

According to a global database, atmospheric fluxes at Hg-enriched sites are positively

correlated with substrate Hg concentrations (Coolbaugh et al., 2002;Gustin et al., 2000;Zehner and Gustin, 2002), but this relationship is not observed at sites with lower background concentrations of soil Hg (Agnan et al., 2016). Our soil Hg fluxes were strongly correlated with soil Hg concentrations at vegetated sites (forests and wetland) of the TFP ($r^2 = 0.97$, $p<0.01$, Fig. S4).

Photo-reduction is a major driver of TGM evasion from the Earth's surface (Howard and Edwards, 2018;Park et al., 2014;Kuss et al., 2018;Song et al., 2018). We found that solar radiation significantly increased TGM fluxes in each plot, especially in the open field (Fig. S2). The fluxes in the wetland (plot C) were less strongly correlated with soil temperature compared to the other plots (r^2=0.09, $p<0.01$ for plot C; and r^2=0.31-0.49, $p<0.001$ for the other plots, Fig. S5). Generally, temperature is an important factor that promotes Hg^0 evasion after its formation from Hg^{2+} by biotic and abiotic processes in soils (Pannu et al., 2014). However, the wetland soil was largely saturated. This condition likely limited soil pore TGM release to the atmosphere, resulting in the weaker correlation between soil temperature and the fluxes.

During the campaign, significant negative correlations were evident between soil moisture and soil-air fluxes of TGM at the five plots (r^2= 0.03−0.39, $p<0.05$ for all, Fig. S6). Generally there is an optimum soil moisture condition that maximizes soil TGM flux (Gustin and Stamenkovic, 2005;Lin et al., 2010;Obrist et al., 2014;Osterwalder et al., 2018;Johnson et al., 2003), which ranges from 60% to 80% of a soil's water holding capacity (Pannu et al., 2014). A laboratory experiment using undisturbed soil collected from the TFP study area showed that increasing soil moisture from 2% to 20% increased the TGM flux 80% at 24 °C (Wang et al., 2014). A second field experiment was conducted to study the effects of higher soil moisture on TGM flux at the TFP, showing that increasing soil moisture gradually decreased the soil Hg emissions over the range of 31−39% (Zhou et al., 2017b). Combining the results of these experiments, the soil Hg fluxes in the forest catchment should increase from low values of soil moisture reaching an optimum in the range of 20-30% and then decreasing with increasing soil moisture above these values. Perennially humid weather results in relatively high soil moisture in the subtropical forest (largely >25% during the campaigns). Considering the relatively high bulk density and low porosity of soil at the TFP (Sørbotten, 2011), soil moisture likely exceeded the optimum range for TGM evasion during the campaigns resulting in significantly negative correlations (Fig. S6).

Soil-air Hg fluxes also showed significant negative correlations with atmospheric TGM

concentrations at the five plots (r^2= 0.03−0.26, $p<0.05$, Fig. S7). According to the two-resistance exchange interface model, the exchange fluxes are controlled by the gradient of TGM concentrations at both interfaces (Zhang et al., 2002), and therefore elevated atmospheric TGM concentrations should decrease the diffusion of soil pore TGM to the atmosphere. These results are consistent with an experiment in this forest, where artificially increasing ambient-air TGM concentrations significantly inhibited soil Hg volatilization (Zhou et al., 2017b).

Diurnal variation in soil-air TGM flux was measured at plot A (Fig. 3). Soil TGM fluxes were well correlated with soil and air temperature ($p<0.01$ for all) and were highly dependent on solar radiation in spring, summer and autumn ($p< 0.01$ for all) but not in winter ($p> 0.05$), which are similar to patterns from other studies (Howard and Edwards, 2018;Osterwalder et al., 2018;Ericksen et al., 2006;Gustin et al., 2002;Johnson et al., 2003). Solar radiation has been shown to promote photochemical reduction of soil-bound Hg and enrich Hg^0 in soil pore gas. This reaction is kinetically enhanced at higher temperatures (Eckley et al., 2015;Gustin et al., 2002;Lin et al., 2010;Zhang et al., 2001). Compared to the other three seasons, the relatively low soil temperature (5.95 °C) may have limited the relationship between soil TGM flux and solar radiation during the winter season.

3.3. Estimation of Hg mass-balance

To investigate the Hg budget of the study site, the flux of Hg inputs (atmospheric Hg deposition) and the flux of Hg outputs from the forest soils (soil-to-air emissions, leaching to surface and groundwater drainage) were calculated (Fig. 1). The total Hg input includes litterfall Hg deposition and throughfall Hg deposition. From previous studies, the annual litterfall and throughfall deposition fluxes of Hg were about 40.5 μg m^{-2} (Zhou et al., 2018b) and 67.5 μg m^{-2} (Luo et al., 2015), respectively, in the study catchment, resulting in an annual Hg input (litterfall + throughfall) to the forest of 108 μg m^{-2}.

The dominant output pathways of Hg from forest were surface and groundwater drainage and the soil-air Hg flux determined from this study. The amount of surface and groundwater runoff, which are assumed to be 25% rainfall amount (Liu, 2005) and 50% throughfall amount, respectively (Luo et al., 2015) and the Hg concentrations in surface and groundwater runoff were 6.2 ng L^{-1} (Wang et al., 2009) and 21.8 ng L^{-1}, respectively (Zhou et al., 2015). The annual output fluxes from

groundwater and surface runoffs were 6.0 and 2.4 μg m^{-2}, respectively, which were roughly estimated according to the Hg concentration in runoffs and their volumes in TFP. Therefore, the total output of Hg (surface runoff + underground runoff + soil-air Hg exchange flux) was approximately 36.4 μg m^{-2} yr^{-1}. The total Hg retention in forest soil (input − output) was estimated to be 71.6 μg m^{-2} yr^{-1}, accounting for 66% of the total Hg deposition. Based on a review of forest Hg in China (Zhou et al., 2018a) and the current study, the THg retention at the subtropical forests ranged from 26.1 to 60.4 μg m^{-2} yr^{-1}, accounted for ranging from 46.6% to 62.8% of THg inputs, suggesting that this forest ecosystem is a net sink for atmospheric Hg.

3.4. Development of empirical models for Hg flux from soils

Predictive models were developed from multivariate regression analysis using the soil-air Hg fluxes and environmental parameters measured at the five plots. Over the last decade, studies have established empirical equations of soil Hg fluxes using one or several parameters, but have not considered air TGM concentrations as a controlling parameter. The empirical equations which utilize different combinations of parameters are summarized in Table S2. Four predictive models were developed for different land cover types investigated: coniferous forest, wetland, broad-leaved forest and open field. Our flux factorial experiments and multivariate response analysis considered quadratic interactions of the environmental parameters that were found to be relevant to soil Hg evasion.

$$F = (a \times S_c) \times [\partial_0 + \partial_1 T + \partial_2 W + \partial_3 L + \partial_4 C_a + \partial_5 (T \times W) + \partial_6 (T \times L) + \partial_7 (T \times C_a) + \partial_8 (W \times L) + \partial_9 (W \times Ca) + \partial_{10} (L \times C_a) + \partial_{11} T^2 + \partial_{12} W^2 + \partial_{13} L^2 + \partial_{14} C_a{}^2] \quad (6)$$

where a is the scaling factor of soil Hg emissions; S_c is soil Hg concentration (ng g^{-1}); W is soil moisture (wt %); L is the fraction of solar radiation attenuated by leaf canopy before reaching to the ground (W m^{-2}), which is parametrized by leaf area index (LAI) in different forest ecosystems (Wang, 2012); C_a is ambient air TGM concentrations (ng m^{-3}); T is soil temperature (°C); and ∂_i is the coefficients of predictors (i = 0−14). The soil Hg concentration was one of the most important parameters driving soil TGM emissions (Gbor et al., 2006;Lin et al., 2010). In this empirical approach soil Hg is multiplied by scaling factor obtained from Fig. S4 ($a = 2.8 \times 10^{-2}$ g m^{-2} hr^{-1}), similar to the approach used by Kikuchi et al. (2013). All the soil parameters were measured in the soil depth of 5 cm.

429 The four different sets of model coefficients were derived separately from the flux data
430 obtained from the field-observation experiments. The number of daily flux observations with
431 corresponding environmental factors used to establish the models were 124, 127, 135 and 102 for
432 the coniferous forest (plot A), the wetland, the broad-leaved forest and the open field, respectively.
433 Regression coefficients for these plots and the whole sub-catchment are shown in Table S3. To
434 simplify the models, ten coefficients were used for each plot based on the principal component
435 analysis (PCA). The estimated mean flux values were 3.92 ± 3.13, 4.20 ± 3.55, −0.88 ± 1.12, 0.14
436 ± 2.38, 23 ± 30 ng m^{-2} hr^{-1}, which were comparable to the measured fluxes of 3.5 ± 4.2, 2.8 ± 3.9,
437 −0.80 ± 5.1, 0.18 ± 4.3 and 24 ± 33 ng m^{-2} hr^{-1} for the plots A to E, respectively.
438 The performance of the models was compared against measured soil flux data (Fig. 4).
439 Normalized Hg flux (predicted using equation 3) agreed well with the measured flux for different
440 ecosystems, with most scatter plots of predicted fluxes falling within the 95% confidence interval
441 (Fig. S8). The cumulative fluxes estimated from the predicted and measured flux was less than 15%
442 different for all land cover types studied. The scatter plots showed strong correlations (r^2 = 0.28 to
443 0.70, Fig. S8) between the measured and predicted fluxes, although the variability of measured
444 fluxes was greater than estimated values. The model was capable of depicting the observed seasonal
445 patterns of soil Hg fluxes with < 5% difference between the measured and predicted values.
446 To date we have had limited opportunity to validate the empirical model predictions. The
447 performance of the empirical model developed for the Masson pine plot A was tested using the data
448 from pine plot B that was not used in developing the empirical model. The model-estimated fluxes
449 of soil TGM for plot B are consistent with measured values using the DFC (Fig. 4). This analysis
450 gives us some confidence in model performance. The multivariate response analysis has improved
451 our ability to estimate soil Hg fluxes. However, further model verification is still needed when
452 additional soil TGM flux data become available, particularly using data from other field study sites.
453
454 **3.5. TGM in Soil Vertical Profiles**
455 Contour plots of soil pore TGM concentrations measured at multiple soil depths and above
456 ground for the four plots (A, B, D and E) are shown in Fig. 5. Mean soil pore TGM concentrations
457 for all depths were significantly higher in the open field (15.8 ± 11.9 ng m^{-3} for plot E), than the
458 Coniferous forest (11.4 ± 10.1 and 12.0 ± 7.83 ng m^{-3} for plots A and B, respectively). These plots

were significantly higher than the broad-leaved forest values (6.73 ± 3.81 ng m^{-3} for plot D). Soil pore TGM concentrations exhibited clear seasonal variations at soil depths at all the study plots. The highest mean TGM concentration was observed in summer, followed by spring and autumn, with the lowest mean concentration in winter. Within each study plot, pore TGM concentrations increased with increases in soil temperature (Table S4), which appears to be an important factor driving the seasonal variation. Soil pore TGM production occurs from the reduction of Hg^{2+} by biotic and abiotic processes. In a laboratory study of boreal forest soils, Pannu et al. (2014) observed that soil Hg converted to Hg^0 via biotic processes was more than five times greater than that derived by abiotic processes, and biotic reduction was more pronounced with temperatures increases. Thus it can be inferred that temperature is an important factor casing in seasonal variation of soil pore TGM concentrations, given limited light penetration to soil depths.

Over the entire campaign at the upper three soil pore sampling depths in each of the four plots, soil moisture was consistently negatively correlated with pore TGM concentrations (Table S4). There is an optimum soil moisture that facilitates pore TGM production, as discussed above. A laboratory study demonstrated increases in soil Hg^0 concentrations with increases in soil moisture from 15% to 60% water filled pore space, with no Hg^0 formation above 80% (Pannu et al., 2014). Additionally, given that soil Hg conversion to Hg^0 is mainly via biotic processes, maximum aerobic microbial activity has been delineated with soil water content equivalent to 60% of a soil's water holding capacity (Breuer et al., 2002;Kiese and Butterbach-Bahl, 2002). Similarly, Obrist et al. (2014) found higher pore TGM concentrations under 25 to 35% soil moisture than for 10 to 20% or 35 to 45% soil moisture in pine forests of California, U.S. At the TFP, more than 95% of soil moisture values exceeded 20%, which may exceed the optimum for soil Hg^0 production, resulting in the inverse correlations.

Sigler and Lee (2006) demonstrated that pore TGM concentrations were significantly correlated with soil Hg concentrations in soil profiles at a forested plot. However, this result is not consistent with our observations. We find that soil pore TGM varies more with varying environmental conditions that soil Hg. We observed vertical TGM gradients in soil during different seasons. In the coniferous forest in spring, the highest pore TGM occurred at a depth of 6 cm. During the other three seasons, the highest mean pore TGM was at 10-cm depth, with values decreasing to the soil surface and the lower layers. In the broad-leaved forest in spring and summer, the highest

489 pore TGM concentrations occurred at the upper soil layer (3cm), and decreased with soil depth. In
490 autumn and winter, the pore TGM concentrations were uniform at the five soil depths. In the open
491 field in summer, the highest pore TGM concentrations occurred at a depth of 6 cm. In autumn and
492 winter, the pore TGM concentrations decreased with depth to 10 cm and were uniform at the three
493 lower depths. With the exception of plots A, D and E in winter, TGM concentrations at 3 cm
494 exceeded values in soil surface air.

495 Soil Hg concentration and SOM were measured at each sampling depth of each plot (Fig. S9).
496 In the forest ecosystem, Hg concentrations were significantly correlated with SOM, with the highest
497 values in the organic layer. Both Hg concentrations and SOM significantly decreased with soil depth,
498 but did not change below depths of 10 cm in the soil profiles. In the open field (plot E), the highest
499 Hg concentrations were found between 10 and 20 cm, with lower Hg concentrations at shallower
500 and deeper depths and Hg concentrations did not vary with SOM likely because of agricultural
501 cultivation. SOM is known to play a central role in the storage and immobilization of Hg in soils
502 (Grigal, 2003;Zhou et al., 2017b). The dominant soil Hg form, Hg^{2+} strongly binds to organic matter
503 through complexation with thiol ligands (Skyllberg et al., 2006). Although much higher Hg
504 concentrations were evident at the upper layers, it seems likely that Hg tightly bound to SOM limits
505 that conversion of Hg^{2+} to Hg^0 by biotic and abiotic processes. Additionally, Schlüter (2000)
506 demonstrated that oxidation of Hg^0 to Hg^{2+} may proceed at a reduction-oxidation potential lower
507 than its half-reaction due to strong binding of Hg^{2+} to organic matter. Our field study in the
508 coniferous forest (Zhou et al., 2017b) and previous sorption studies (Eckley et al., 2011b;Fang, 1978)
509 also have shown that Hg^0 is adsorbed rapidly to surface soils under high air Hg^0 exposure. In the
510 coniferous forest, the mean SOM decreased from 137.6 g kg^{-1} at the surface to 58.0 g kg^{-1} at depth,
511 while the pore TGM concentrations increased from 9.44 to 14.63 ng m^{-3} in the interval of 3 cm.
512 Thus, Hg^0 produced at surface layers or transported from deeper soil layers may be re-oxidized or
513 absorbed by SOM in the surface soil. Although a similar SOM pattern was evident in the soil profiles
514 of the broad-leaved forest, the highest pore TGM concentrations occurred in surface soils. The
515 surface SOM of the broad-leaved forest (67.9 g kg^{-1} at 3 cm) was half the value of the coniferous
516 forest (137.6 g kg^{-1}), while the soil Hg concentration was highest at this surface layer. The higher
517 Hg to SOM ratio at the broad-leaved forest may have contributed to greater surface pore TGM
518 production, due to less immobilization of Hg^0 associated with the lower concentrations of SOM.

519 Lower pore TGM concentrations in the broad-leaved forest than the coniferous forest may also
520 be due to local differences in porosity, SOM and Hg concentrations. In the open field, the vertical
521 profiles of pore TGM may be influenced by direct solar radiation that increases soil temperature in
522 the upper layers. When surface soil temperature in autumn and winter decrease, the vertical TGM
523 profile is dominated by soil Hg concentration. For example, higher soil pore TGM in the surface
524 soil layer (24 ng m^{-3}) in summer (mean soil temperature = 24.1 ℃) is significantly higher than the
525 values in autumn and winter (9 ng m^{-3}, mean soil temperature = 10.4 ℃). In contrast, the vertical
526 pattern of soil pore TGM concentrations was similar in the autumn and winter seasons (Fig. 5 and
527 Fig. S9). In all plots during all four seasons, comparable TGM concentrations were observed
528 between 20 and 50 cm, which may be due to comparable physicochemical properties in lower
529 mineral horizons (e.g. Hg concentrations, SOM, Fig. S9).
530 Although other studies have shown different TGM patterns than observed in our study (Moore
531 and Castro, 2012;Obrist et al., 2014;Sigler and Lee, 2006), our measurements seem to support
532 observations of TGM distributions. For example, the soil pore TGM concentrations were highest
533 and most variable in the O- and upper A-horizons of forest soils, with soil moisture, temperature
534 and SOM significantly affecting TGM concentrations. Soil pore TGM concentrations at the TFP
535 were much higher than values reported in previous studies, which have shown concentrations
536 ranging from the detection limit to 8 ng m^{-3} in upper soils and were generally less than 2 ng m^{-3}
537 from 20 to 50 cm of the soil profile (Moore and Castro, 2012;Sigler and Lee, 2006). Sigler and Lee
538 (2006) and Obrist et al. (2014) observed the highest pore TGM concentrations in the upper organic
539 soil and litter layers, which is inconsistent with our observation of maximum TGM concentrations
540 in the upper mineral soil (depth 6−10 cm) in the coniferous forest. Previous studies have also shown
541 the highest pore TGM concentrations observed in the upper mineral soil layers (Obrist et al., 2014).
542 Our observations and the above studies show a near-surface source of TGM from soil evading to
543 the atmosphere. Observations of soil pore TGM concentrations decreasing in lower layers supports
544 a TGM sink in mineral soils. Obrist et al. (2014) defined an Hg^0 immobilization concept for soils,
545 in which pore TGM concentrations in lower horizons are below values in the upper horizons. In the
546 forest plots at the TFP, the annual average soil pore TGM concentrations at 10, 20 and 30 cm were
547 all below concentrations in the upper horizons; suggesting immobilization of TGM in the mineral
548 soil, a pattern consistent with a study of two pine forests in California, U.S. (Obrist et al., 2014).

549 However, for the open field in our study, TGM formation mostly occurred in mineral soils coincident
550 with higher soil Hg concentrations in the mineral horizons as stated above, which may facilitate the
551 mineral pore TGM diffusion to surface soil horizon and the emission flux. Another major objective
552 of our soil pore TGM study was to investigate the relationship between TGM in vertical soil pore
553 profiles and the ultimate diffusion of TGM from the soil surface. No relationship was found between
554 soil pore TGM flux and soil pore TGM concentrations at 20 or 50 cm. Sigler and Lee (2006) showed
555 that Hg emissions originated from shallow (5 cm) depths in forest soils due to highest soil pore
556 TGM produced in surface horizons. In our study, soil TGM fluxes were strongly correlated with the
557 gradient between soil pore concentrations at 2, 5 and 10 cm depths and the atmosphere (Fig. S10).
558 TGM concentrations were highest at these surface depths and values decreased with greater depth,
559 suggesting that production and subsequent emission of Hg from soil is derived from the upper 10-
560 cm depths.

561 We also investigated the role of vertical profiles of pore TGM in diffusion from the soil column.
562 In Eg. 5, F can be derived from the diffusion of pore TGM or from photochemical reduction of Hg^{2+}
563 on soil surface during daytime. We estimated the diffusion coefficient between the soil at 3 cm and
564 the atmosphere during daytime ($D_{s\ day}$), nighttime ($D_{s\ night}$) and for the entire day ($D_{s\ day+\ night}$). The
565 estimated $D_{s\ day}$, $D_{s\ night}$ and $D_{s\ day+\ night}$ were 0.015, 0.013 and 0.014 $m^2\ hr^{-1}$ for plot A and 0.0098,
566 0.0096 and 0.0097 $m^2\ hr^{-1}$ for plot B in the coniferous forest, and 0.010, 0.0076 and 0.0079 $m^2\ hr^{-1}$
567 for plot C in the broad-leaved forest, respectively. However, in the open field, TGM diffusion
568 coefficient was found to be up to 10 times higher in the daytime ($D_{s\ day}$: 0.099 $m^2\ hr^{-1}$) than for
569 nighttime ($D_{s\ night}$: 0.0095 $m^2\ hr^{-1}$), with day and night ($D_{s\ day+night}$: 0.0408 $m^2\ hr^{-1}$). Note that, in the
570 open field, the Ds night was comparable to those in forest plots, but the D_s day was significantly
571 higher. During daytime, especially in the open field, stronger solar radiation increased the reduction
572 of Hg^{2+} on the soil surface and therefore resulted in a higher flux (higher D_s). Photo-reduction of
573 Hg^{2+} in soil is important source of the Hg^0 emission, which may overestimate the diffusivity of
574 TGM during daytime (Eckley et al., 2011a;Eckley et al., 2011b). Our results suggest that the
575 formation of Hg^0 in the surface soil exposed to solar radiation likely led to an overestimation of Ds
576 in soil. Therefore, we assumed that Ds night can be used represent the local diffusion coefficient
577 (Ds) (Fig. 6) and applied in future model development.

578 Physicochemical properties of soils have a significant effect on the pore gas production and

transport, especially porosity and humidity (Prajapati and Jacinthe, 2014;Ryzhakova, 2014). In the same coniferous stand, the soil TGM diffusion coefficient was much higher at plot A (0.013 m^2 hr^{-1}) than plot B (0.0.0096 m^2 hr^{-1}). This difference may be related to the higher SOM at plot B. The higher SOM could immobilize TGM in the upper soil as discussed above, mitigating pore TGM diffusion to the atmosphere. Ryzhakova (2014) found that the D_s of radon ranged from 0.00050 to 0.0088 m^2 hr^{-1} for natural soils and Prajapati and Jacinthe (2014) determined that the D_s for sulphur hexafluoride for the peat cores ranged between 0.00032 to 0.0044 m^2 hr^{-1}. These values are comparable with the D_s values of Hg in our study.

4. Conclusions and study implications

Through multi-plot measurements over 130 days, we were able to reduce the uncertainty of soil-atmosphere TGM fluxes at the catchment scale and improve understanding of how landscape attributes contribute to the variability in soil Hg evasion. Empirical models of soil-air exchange fluxes were developed from multivariate regression analysis using the Hg fluxes measured by the DFC and environmental factors for different landscape conditions in a forest catchment. The observed DFC fluxes were significantly correlated to the first-order and second-order terms of environmental factors, including soil Hg concentration, soil moisture, solar radiation, TGM concentration in ambient air, and soil temperature. In particular, we found that atmospheric TGM concentrations in ambient air at TFP significantly affect TGM diffusion form soil pore as suggested by a two-resistance exchange interface model.

The developed model can be used to examine how soil Hg fluxes may be impacted by changes in environmental conditions such as temperature, soil moisture or concentrations of atmospheric TGM. For example, if the atmospheric TGM decreased to a uniform 0.1 ng m^{-3}, the Hg area-weighted emission flux is projected to increase up to 5.0% in the forest and 0.5% in the open field, respectively. The empirical models presented in this study demonstrate a promising approach to improve estimates of Hg exchange between the atmosphere and soil. Additional data from additional sites which represent wider range of substrates and environmental conditions in different terrestrial ecosystems are needed to verify the empirically modeling framework we propose.

Another implication of our results is that Hg in upper mineral layers would migrate to lower mineral horizons through pore TGM diffusion, although this pathway may small compared with

609 rainwater infiltration and immobilization (Jiskra et al., 2015). For instance, throughfall Hg
610 deposition was 67.5 μg m^{-2} yr^{-1} in the coniferous forest in our study area (Luo et al., 2015) and the
611 percolation of Hg via soil solution through the surface litter layer into the mineral soil layer has been
612 estimated at 33 μg m^{-2} yr^{-1} (Schwesig and Matzner, 2001). Thus, transport and immobilization of
613 soil pore TGM to the lower mineral soil is likely to be much smaller than by the drainage pathway.
614 In each season, soil Hg flux was strongly correlated with pore TGM concentrations at 3 cm depth
615 and less strongly correlated than concentrations at other depths, suggesting that reduction and
616 terrestrial Hg^0 losses would occur within the upper surface soil horizons, with limited loss from
617 deeper mineral soils. The large Hg pools in mineral soils (accounting for 94.1% of the total over
618 0−40 cm) (Zhou et al., 2016) were not only derived from soil water percolation but also with a
619 contribution from TGM diffusion from upper soils. Compared to Hg concentrations of mountain
620 yellow earth soil measured in 1980s in Chongqing China (59 ng g^{-1}) (Chen, 1982), the average Hg
621 concentration in the mineral horizons (85 ng g^{-1}, 6~50 cm) in our study increased about 44%.
622
623 ***Author contributions.*** JZ performed the field observation. ZWW and XSZ designed the
624 experiments and assisted with the initial instrument installation. ZWW, CTD, XSZ and CJL assisted
625 with scientific analysis and revised manuscript. JZ prepared the manuscript with significant
626 contributions from all of co-authors.
627
628 ***Competing interests.*** The authors declare that they have no conflict of interest.
629
630 **ACKNOWLEDGEMENTS**
631 This work was funded by the National Key Research and Development Program of China
632 (2017YFC0210105), the National Basic Research Program of China (973 Program;
633 2013CB430002), and Natural Science Foundation of China (No. 41673113 and No.41371461). The
634 authors would like to thank Mingquan Zou for his assistance in field works.
635
636 **References**
637 Agnan, Y., Le, D. T., Moore, C., Edwards, G., and Obrist, D.: New constraints on terrestrial surface-
638 atmosphere fluxes of gaseous elemental mercury using a global database, Environmental Science
639 & Technology, 50, 507−524, 10.1021/acs.est.5b04013, 2016.

Beckers, F., and Rinklebe, J.: Cycling of mercury in the environment: Sources, fate, and human health implications: A review, Critical Reviews in Environmental Science and Technology, 47, 693-794, 10.1080/10643389.2017.1326277, 2017.

Blackwell, B. D., Driscoll, C. T., Maxwell, J. A., and Holsen, T. M.: Changing climate alters inputs and pathways of mercury deposition to forested ecosystems, Biogeochemistry, 119, 215-228, 10.1007/s10533-014-9961-6, 2014.

Breuer, L., Kiese, R., and Butterbachbahl, K.: Temperature and moisture effects on nitrification rates in tropical rain-forest soils, Soil Science Society of America Journal, 66, 399-402, 2002.

Briggs, C., and Gustin, M. S.: Building upon the Conceptual Model for Soil Mercury Flux: Evidence of a Link Between Moisture Evaporation and Hg Evasion, Water Air and Soil Pollution, 224, 10.1007/s11270-013-1744-5, 2013.

Carpi, A., and Lindberg, S. E.: Application of a Teflon (TM) dynamic flux chamber for quantifying soil mercury flux: Tests and results over background soil, Atmospheric Environment, 32, 873-882, 10.1016/s1352-2310(97)00133-7, 1998.

Chen, Y.: Distribution of mercury in soils in Chongqing area, Chongqing Environmental Protection, 4, 106-113. In Chinese., 1982.

Chen, Y., Yin, Y., Shi, J., Liu, G., Hu, L., Liu, J., Cai, Y., and Jiang, G.: Analytical methods, formation, and dissolution of cinnabar and its impact on environmental cycle of mercury, Critical Reviews in Environmental Science and Technology, 47, 2415-2447, 10.1080/10643389.2018.1429764, 2017.

Choi, H. D., and Holsen, T. M.: Gaseous mercury fluxes from the forest floor of the Adirondacks, Environmental Pollution, 157, 592, 2009.

Coolbaugh, M. F., Gustin, M. S., and Rytuba, J. J.: Annual emissions of mercury to the atmosphere from natural sources in Nevada and California, Environmental Geology, 42, 338-349, 10.1007/s00254-002-0557-4, 2002.

Eckley, C. S., Gustin, M., Lin, C. J., Li, X., and Miller, M. B.: The influence of dynamic chamber design and operating parameters on calculated surface-to-air mercury fluxes, Atmospheric Environment, 44, 194-203, 10.1016/j.atmosenv.2009.10.013, 2010.

Eckley, C. S., Gustin, M., Marsik, F., and Miller, M. B.: Measurement of surface mercury fluxes at active industrial gold mines in Nevada (USA), Science of the Total Environment, 409, 514-522, 10.1016/j.scitotenv.2010.10.024, 2011a.

Eckley, C. S., Gustin, M., Miller, M. B., and Marsik, F.: Scaling non-point-source mercury emissions from two active industrial gold mines: Influential variables and annual emission estimates, Environmental Science & Technology, 45, 392-399, 2011b.

Eckley, C. S., Blanchard, P., Mclennan, D., Mintz, R., and Sekela, M.: Soil–air mercury flux near a large industrial emission source before and after closure (Flin Flon, Manitoba, Canada), Environmental Science & Technology, 49, 9750-9757, 2015.

Engle, M. A., Gustin, M. S., Lindberg, S. E., Gertler, A. W., and Ariya, P. A.: The influence of ozone on atmospheric emissions of gaseous elemental mercury and reactive gaseous mercury from substrates, Atmospheric Environment, 39, 7506-7517, 10.1016/j.atmosenv.2005.07.069, 2005.

Ericksen, J. A., Gustin, M. S., Xin, M., Weisberg, P. J., and Fernandez, G. C. J.: Air-soil exchange of mercury from background soils in the United States, Science of the Total Environment, 366, 851-863, 10.1016/j.scitotenv.2005.08.019, 2006.

Fang, S. C.: Sorption and transformation of mercury vapor by dry soil, Environmental Science & Technology, 12, 285-288, 1978.

Fu, X. W., Zhang, H., Yu, B., Wang, X., Lin, C. J., and Feng, X. B.: Observations of atmospheric mercury in China: a critical review, Atmospheric Chemistry and Physics, 15, 9455-9476, 10.5194/acp-15-9455-2015, 2015.

Gbor, P. K., Wen, D., Meng, F., Yang, F., Zhang, B., and Sloan, J. J.: Improved model for mercury emission, transport and deposition, Atmospheric Environment, 40, 973-983, 2006.

Grigal, D. F.: Mercury sequestration in forests and peatlands: a review, Journal of Environmental Quality, 32, 393, 2003.

Gustin, M. S., Jr, G. E. T., and Maxey, R. A.: Effect of temperature and air movement on the flux of elemental mercury from substrate to the atmosphere, Journal of Geophysical Research Atmospheres, 102, 3891-3898, 1997.

Gustin, M. S., Lindberg, S. E., Austin, K., Coolbaugh, M., Vette, A., and Zhang, H.: Assessing the contribution of natural sources to regional atmospheric mercury budgets, Science of the Total Environment, 259, 61-71, 10.1016/s0048-9697(00)00556-8, 2000.

Gustin, M. S., Biester, H., and Kim, C. S.: Investigation of the light-enhanced emission of mercury from naturally enriched substrates, Atmospheric Environment, 36, 3241-3254, 2002.

Gustin, M. S.: Are mercury emissions from geologic sources significant? A status report, Science of the Total Environment, 304, 153, 2003.

Gustin, M. S., and Stamenkovic, J.: Effect of watering and soil moisture on mercury emissions from soils, Biogeochemistry, 76, 215-232, 2005.

Howard, D., and Edwards, G. C.: Mercury fluxes over an Australian alpine grassland and observation of nocturnal atmospheric mercury depletion events, Atmospheric Chemistry and Physics, 18, 129-142, 10.5194/acp-18-129-2018, 2018.

Jiskra, M., Wiederhold, J. G., Skyllberg, U., Kronberg, R. M., Hajdas, I., and Kretzschmar, R.: Mercury deposition and re-emission pathways in boreal forest soils investigated with hg isotope signatures, Environmental Science & Technology, 49, 7188-7196, 2015.

Johnson, D. W., Benesch, J. A., Gustin, M. S., Schorran, D. S., Lindberg, S. E., and Coleman, J. S.: Experimental evidence against diffusion control of Hg evasion from soils, Science of the Total Environment, 304, 175-184, 10.1016/s0048-9697(02)00567-3, 2003.

Kiese, R., and Butterbach-Bahl, K.: N2O and CO2 emissions from three different tropical forest sites in the wet tropics of Queensland, Australia, Soil Biology & Biochemistry, 34, 975-987, 2002.

Kikuchi, T., Ikemoto, H., Takahashi, K., Hasome, H., and Ueda, H.: Parameterizing soil emission and atmospheric oxidation-reduction in a model of the global biogeochemical cycle of mercury, Environmental Science & Technology, 47, 12266-12274, 2013.

Kocman, D., and Horvat, M.: A laboratory based experimental study of mercury emission from contaminated soils in the River Idrijca catchment, Atmospheric Chemistry and Physics, 10, 1417-1426, 2010.

Kumari, A., Kumar, B., Manzoor, S., and Kulshrestha, U.: Status of Atmospheric Mercury Research in South Asia: A Review, Aerosol and Air Quality Research, 15, 1092-1109, 10.4209/aaqr.2014.05.0098, 2015.

Kuss, J., Krueger, S., Ruickoldt, J., and Wlost, K.-P.: High-resolution measurements of elemental mercury in surface water for an improved quantitative understanding of the Baltic Sea as a source of atmospheric mercury, Atmospheric Chemistry and Physics, 18, 4361-4376, 10.5194/acp-18-4361-2018, 2018.

Kyllonen, K., Hakola, H., Hellen, H., Korhonen, M., and Verta, M.: Atmospheric Mercury Fluxes in a

Southern Boreal Forest and Wetland, Water Air and Soil Pollution, 223, 1171-1182, 10.1007/s11270-011-0935-1, 2012.

Larssen, T., de Wit, H. A., Wiker, M., and Halse, K.: Mercury budget of a small forested boreal catchment in southeast Norway, Science of the Total Environment, 404, 290-296, 10.1016/j.scitotenv.2008.03.013, 2008.

Li, Z. G., Feng, X., Li, P., Liang, L., Tang, S. L., Wang, S. F., Fu, X. W., Qiu, G. L., and Shang, L. H.: Emissions of air-borne mercury from five municipal solid waste landfills in Guiyang and Wuhan, China, Atmospheric Chemistry & Physics, 10, 3353-3364, 2010.

Lin, C. J., Gustin, M. S., Singhasuk, P., Eckley, C., and Miller, M.: Empirical models for estimating mercury flux from soils, Environmental Science & Technology, 44, 8522-8528, 2010.

Lindberg, S. E., Hanson, P. J., Meyers, T. P., and Kim, K. H.: Air/surface exchange of mercury vapor over forests - The need for a reassessment of continental biogenic emissions, Atmospheric Environment, 32, 895-908, 10.1016/s1352-2310(97)00173-8, 1998.

Liu, H.: Dynamics of soil properties and the effects factors among secondary successive communities in Mt. Jinyun, Doctor's dissertation, Southwest Agricultural University, Chongqing, pp. 1-117 pp., 2005.

Luo, Y., Duan, L., Xu, G., and Hao, J.: Inhibition of mercury release from forest soil by high atmospheric deposition of Ca(2)(+) and SO(4)(2)(-), Chemosphere, 134, 113-119, 10.1016/j.chemosphere.2015.03.081, 2015.

Ma, M., Wang, D., Sun, R., Shen, Y., and Huang, L.: Gaseous mercury emissions from subtropical forested and open field soils in a national nature reserve, southwest China, Atmospheric Environment, 64, 116-123, 2013.

Mason, R. P., Fitzgerald, W. F., and Morel, F. M. M.: The biogeochemical cycling of elemental mercury: Anthropogenic influences, Geochimica Et Cosmochimica Acta, 58, 3191-3198, 1994.

Moore, C. W., Castro, M. S., and Brooks, S. B.: A simple and accurate method to measure total gaseous mercury concentrations in unsaturated soils, Water Air & Soil Pollution, 218, 11-11, 2011.

Moore, C. W., and Castro, M. S.: Investigation of factors affecting gaseous mercury concentrations in soils, Science of the Total Environment, 419, 136-143, 2012.

Obrist, D., Faïn, X., and Berger, C.: Gaseous elemental mercury emissions and CO(2) respiration rates in terrestrial soils under controlled aerobic and anaerobic laboratory conditions, Science of the Total Environment, 408, 1691-1700, 2010.

Obrist, D.: Mercury distribution across 14 U.S. forests. Part II: Patterns of methyl mercury concentrations and areal mass of total and methyl mercury, Environmental Science & Technology, 46, 7434, 2012.

Obrist, D., Pokharel, A. K., and Moore, C.: Vertical profile measurements of soil air suggest immobilization of gaseous elemental mercury in mineral soil, Environmental Science & Technology, 48, 2242, 2014.

Obrist, D., Agnan, Y., Jiskra, M., Olson, C. L., Colegrove, D. P., Hueber, J., Moore, C. W., Sonke, J. E., and Helmig, D.: Tundra uptake of atmospheric elemental mercury drives Arctic mercury pollution, Nature, 547, 201-+, 10.1038/nature22997, 2017.

Obrist, D., Kirk, J. L., Zhang, L., Sunderland, E. M., Jiskra, M., and Selin, N. E.: A review of global environmental mercury processes in response to human and natural perturbations: Changes of emissions, climate, and land use, Ambio, 47, 116-140, 10.1007/s13280-017-1004-9, 2018.

Osterwalder, S., Sommar, J., Akerblom, S., Jocher, G., Fritsche, J., Nilsson, M. B., Bishop, K., and Alewell, C.: Comparative study of elemental mercury flux measurement techniques over a

772 Fennoscandian boreal peatland, Atmospheric Environment, 172, 16-25,
773 10.1016/j.atmosenv.2017.10.025, 2018.
774 Outridge, P. M., Mason, R. P., Wang, F., Guerrero, S., and Heimburger-Boavida, L. E.: Updated global
775 and oceanic mercury budgets for the united nations global mercury assessment 2018, Environmental
776 Science & Technology, 52, 11466-11477, 10.1021/acs.est.8b01246, 2018.
777 Pan, L., Lin, C.-J., Carmichael, G. R., Streets, D. G., Tang, Y., Woo, J.-H., Shetty, S. K., Chu, H.-W., Ho,
778 T. C., Friedli, H. R., and Feng, X.: Study of atmospheric mercury budget in East Asia using STEM-
779 Hg modeling system, Science of the Total Environment, 408, 3277-3291,
780 10.1016/j.scitotenv.2010.04.039, 2010.
781 Pannu, R., Siciliano, S. D., and O'Driscoll, N. J.: Quantifying the effects of soil temperature, moisture
782 and sterilization on elemental mercury formation in boreal soils, Environmental Pollution, 193, 138,
783 2014.
784 Park, S. Y., Holsen, T. M., Kim, P. R., and Han, Y. J.: Laboratory investigation of factors affecting
785 mercury emissions from soils, Environmental Earth Sciences, 72, 2711-2721, 2014.
786 Peleg, M., Tas, E., Matveev, V., Obrist, D., Moore, C. W., Gabay, M., and Luria, M.: Observational
787 evidence for involvement of nitrate radicals in nighttime oxidation of mercury, Environmental
788 Science & Technology, 49, 14008, 2015.
789 Prajapati, P., and Jacinthe, P. A.: Methane oxidation kinetics and diffusivity in soils under conventional
790 tillage and long-term no-till, Geoderma, s 230–231, 161-170, 2014.
791 Renner, R.: Newly deposited mercury may be more bioavailable, Environmental Science & Technology,
792 36, 226A-227A, 10.1021/es0223224, 2002.
793 Risch, M. R., DeWild, J. F., Gay, D. A., Zhang, L., Boyer, E. W., and Krabbenhoft, D. P.: Atmospheric
794 mercury deposition to forests in the eastern USA, Environmental Pollution, 228, 8-18,
795 10.1016/j.envpol.2017.05.004, 2017.
796 Ryzhakova, N. K.: A new method for estimating the coefficients of diffusion andemanation of radon in
797 the soil, Journal of Environmental Radioactivity, 135, 63-66, 2014.
798 Schlüter, K.: Review: evaporation of mercury from soils. An integration and synthesis of current
799 knowledge, Environmental Geology, 39, 249-271, 2000.
800 Schwesig, D., and Matzner, E.: Dynamics of mercury and methylmercury in forest floor and runoff of a
801 forested watershed in central Europe, Biogeochemistry, 53, 181-200, 2001.
802 Selvendiran, P., Driscoll, C., T, Bushey, J. T., and Montesdeoca, M. R.: Wetland influence on mercury
803 fate and transport in a temperate forested watershed, Environmental Pollution, 154, 46-55, 2008.
804 Sigler, J. M., and Lee, X.: Gaseous mercury in background forest soil in the northeastern United States,
805 Journal of Geophysical Research Biogeosciences, 111, G02007, 10.1029/2005JG000106, 2006.
806 Skyllberg, U., Bloom, P. R., Qian, J., Lin, C. M., and Bleam, W. F.: Complexation of mercury(II) in soil
807 organic matter: EXAFS evidence for linear two-coordination with reduced sulfur groups,
808 Environmental Science & Technology, 40, 4174-4180, 10.1021/es0600577, 2006.
809 Song, S., Angot, H., Selin, N. E., Gallee, H., Sprovieri, F., Pirrone, N., Helmig, D., Savarino, J., Magand,
810 O., and Dommergue, A.: Understanding mercury oxidation and air-snow exchange on the East
811 Antarctic Plateau: a modeling study, Atmospheric Chemistry and Physics, 18, 15825-15840,
812 10.5194/acp-18-15825-2018, 2018.
813 Sørbotten, L. E.: Hill slope unsaturated flowpaths and soil moisture variability in a forested catchment
814 in Southwest China, MD, Department of Plant and Environmental Sciences, University of Life
815 Sciences, 2011.

816 Teixeira, D. C., Lacerda, L. D., and Silva-Filho, E. V.: Foliar mercury content from tropical trees and its
817 correlation with physiological parameters in situ, Environmental Pollution, 242, 1050-1057,
818 10.1016/j.envpol.2018.07.120, 2018.
819 Wang, Q., Luo, Y., Du, B., Ye, Z., and Duan, L.: Influencing factors of mercury emission flux from forest
820 soil at tieshanping,chongqing, Environmental Science, 35, 1922-1927, 2014.
821 Wang, S., Feng, X., Qiu, G., Fu, X., and Wei, Z.: Characteristics of mercury exchange flux between soil
822 and air in the heavily air-polluted area, eastern Guizhou, China, Atmospheric Environment, 41,
823 5584-5594, 2007.
824 Wang, X., Bao, Z., Lin, C.-J., Yuan, W., and Feng, X.: Assessment of global mercury deposition through
825 litterfall, Environmental Science & Technology, 50, 8548-8557, 10.1021/acs.est.5b06351, 2016.
826 Wang, X., Lin, C.-J., Feng, X., Yuan, W., Fu, X., Zhang, H., Wu, Q., and Wang, S.: Assessment of regional
827 mercury deposition and emission outflow in mainland China, Journal of Geophysical Research-
828 Atmospheres, 123, 9868-9890, 10.1029/2018jd028350, 2018.
829 Wang, Y.: Characteristics of stand structure and hydrological function of damaged Masson pine forests
830 in the acid rain region of Chongqing, MD, Chinese Academy of Forestry, 2012.
831 Wang, Z., Zhang, X., Xiao, J., Zhijia, C., and Yu, P.: Mercury fluxes and pools in three subtropical
832 forested catchments, southwest China, Environmental Pollution, 157, 801-808,
833 10.1016/j.envpol.2008.11.018, 2009.
834 Wright, L. P., Zhang, L., and Marsik, F. J.: Overview of mercury dry deposition, litterfall, and throughfall
835 studies, Atmospheric Chemistry and Physics, 16, 13399-13416, 10.5194/acp-16-13399-2016, 2016.
836 Xin, M., and Gustin, M. S.: Gaseous elemental mercury exchange with low mercury containing soils:
837 Investigation of controlling factors, Applied Geochemistry, 22, 1451-1466, 2007.
838 Zarate-Valdez, J. L., Zasoski, R. J., and Lauchli, A.: Short-term effects of moisture content on soil
839 solution pH and soil Eh, Soil Science, 171, 423-431, 10.1097/01.ss.0000222887.13383.08, 2006.
840 Zehner, R. E., and Gustin, M. S.: Estimation of mercury vapor flux from natural substrate in Nevada,
841 Environmental Science & Technology, 36, 4039-4045, 10.1021/es015723c, 2002.
842 Zhang, H., Lindberg, S. E., Marsik, F. J., and Keeler, G. J.: Mercury air/surface exchange kinetics of
843 background soils of the tahquamenon river watershed in the Michigan Upper Peninsula, Water Air
844 & Soil Pollution, 126, 151-169, 2001.
845 Zhang, H., Lindberg, S. E., Barnett, M. O., Vette, A. F., and Gustin, M. S.: Dynamic flux chamber
846 measurement of gaseous mercury emission fluxes over soils. Part 1: simulation of gaseous mercury
847 emissions from soils using a two-resistance exchange interface model, Atmospheric Environment,
848 36, 835-846, 2002.
849 Zhou, J., Feng, X., Liu, H., Zhang, H., Fu, X., Bao, Z., Wang, X., and Zhang, Y.: Examination of total
850 mercury inputs by precipitation and litterfall in a remote upland forest of Southwestern China,
851 Atmospheric Environment, 81, 364-372, 10.1016/j.atmosenv.2013.09.010, 2013.
852 Zhou, J., Wang, Z., Zhang, X., and Chen, J.: Distribution and elevated soil pools of mercury in an acidic
853 subtropical forest of southwestern China, Environmental Pollution, 202, 187-195,
854 10.1016/j.envpol.2015.03.021, 2015.
855 Zhou, J., Wang, Z., Sun, T., Zhang, H., and Zhang, X.: Mercury in terrestrial forested systems with highly
856 elevated mercury deposition in southwestern China: The risk to insects and potential release from
857 wildfires, Environmental Pollution, 212, 188-196, 10.1016/j.envpol.2016.01.003, 2016.
858 Zhou, J., Wang, Z., Zhang, X., and Gao, Y.: Mercury concentrations and pools in four adjacent coniferous
859 and deciduous upland forests in Beijing, China, Journal of Geophysical Research Biogeosciences,

122, 1260-1274, 2017a.
Zhou, J., Wang, Z., Zhang, X., and Sun, T.: Investigation of factors affecting mercury emission from subtropical forest soil: A field controlled study in southwestern China, Journal of Geochemical Exploration, 176, 128-135, 10.1016/j.gexplo.2015.10.007, 2017b.
Zhou, J., Du, B., Wang, Z., Shang, L., and Zhou, J.: Mercury fluxes, budgets and pools in forest ecosystems of China: A critical review, Atmospheric Chemistry and Physics Discussions, 1-40, 10.5194/acp-2017-794, 2018a.
Zhou, J., Wang, Z., and Zhang, X.: Deposition and fate of mercury in litterfall, litter, and soil in coniferous and broad-leaved forests, Journal of Geophysical Research-Biogeosciences, 123, 2590-2603, 10.1029/2018jg004415, 2018b.

872 **Table 1.** Locations and detailed measurements of soil-air TGM flux, soil pore TGM concentrations and environmental parameters at five plots in the subtropical forest.

Plots	Locations	Soil surface TGM (ng m^{-3})	Soil pore TGM (ng m^{-3})					Flux	Soil Hg concentration (ng g^{-1})	Soil moisture (%)	Soil temperature (℃)	Solar radiation (W m^{-2})
			3 cm	6 cm	10 cm	20 cm	50 cm					
Plot A	Top-slope of coniferous forest	3.6±1.3	8.4±7.9	9.8±8.7	13.0±12.2	12.5±10.2	13.0±9.8	2.8 ± 3.9	219±15	0.3±0.1	16.8±7.6	39.9±27.5
Plot B	Middle-slope of the coniferous forest	3.8±1.3	10.0±6.2	11.9±6.1	15.1±9.8	12.7±7.9	10.4±7.4	3.5 ± 4.2	263±22	0.4±0.1	16.9±7.7	40.2±27.5
Plot C	Wetland	3.7±1.4						-0.80 ± 5.1	96±43	0.3±0.1	16.7±7.5	20.5±27.9
Plot D	Broad-leaved forest	3.3±1.4	8.0±4.8	7.1±4.3	6.2±3.4	6.2±2.0	5.8±2.8	0.18 ± 4.3	156±17	0.3±0.1	16.9±7.6	20.3±27.9
Plot E	Open field (bare soil)	4.1±1.7	12.9±11.0	18.5±16.9	14.1±9.2	17.0±9.7	16.6±10.1	24 ± 33	159±18	0.3±0.1	18.3±8.5	98.0±138.4

873

874

Figure Captions:

Fig. 1. Location of the five sampling plots and the estimation of Hg mass-balance at the TFP subtropical forest (blue square: flux sampling site; spiral line: Soil pore TGM sampling site). Litterfall Hg deposition was determined from Zhou et al. (2018b); throughfall Hg deposition was obtained from Luo et al. (2015); surface runoff (SR) Hg flux was obtained from Zhou et al. (2015); wet Hg deposition was obtained from Wang et al. (2009); soil Hg pools were obtained from Zhou et al. (2016); UR represents groundwater drainage.

Fig. 2. Mean and standard deviation of soil-air TGM fluxes at the five plots for the four seasons and annual values during the study. Plots A, B and C were located in the coniferous forest, plot D was in the broad-leaved forest, and plot E was in the open field. The number of flux observations in spring, summer, autumn and winter were 62, 92, 66 and 43, respectively.

Fig. 3. The daily patterns of soil Hg fluxes with meteorological parameters in spring (a), summer (b), autumn (c) and winter (d) at the coniferous forest.

Fig. 4. Comparison between model-predicted and DFC-measured fluxes of Hg for the five plots. DFC-measured flux is a daily flux from averaged daytime and night values. Plot A was positioned on the top of the hill slope; plot B was in the middle of the hill slope; plot C was in the wetland within a coniferous forest; plot D was in broad-leaved (evergreen) forest and plot E is in open field.

Fig. 5. Contour plots of soil pore TGM concentrations which in order are plots A, B, D and E. Plots were created based on daytime and night pore TGM measurements combining soil surface (3 cm) and 5 soil layers (3 cm, 6cm, 10cm, 20cm and 50cm).

Fig. 6. Scatter plots and linear regressions between soil-air fluxes and the gradient of TGM concentration divided the distance between soil pore TGM at 3 cm (*Cs*) and the atmosphere above the plot (*Ca*) based on the two-resistance exchange interface model. The relationships were based on night flux and soil TGM measurements, and were significant at the respective plots ($p<0.05$).

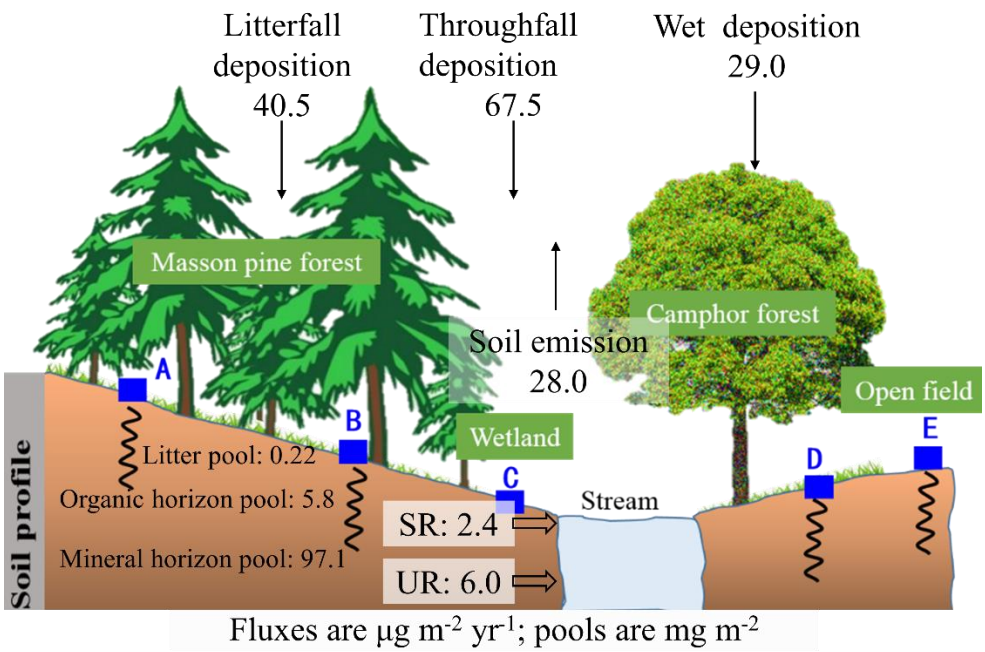

Fig. 1. Location of the five sampling plots and the estimation of Hg mass-balance at the TFP subtropical forest (blue square: flux sampling site; spiral line: Soil pore TGM sampling site). Litterfall Hg deposition was determined from Zhou et al. (2018b); throughfall Hg deposition was obtained from Luo et al. (2015); surface runoff (SR) Hg flux was obtained from Zhou et al. (2015); wet Hg deposition was obtained from Wang et al. (2009); soil evasion was obtained from this study; soil Hg pools were obtained from Zhou et al. (2016); UR represents groundwater drainage.

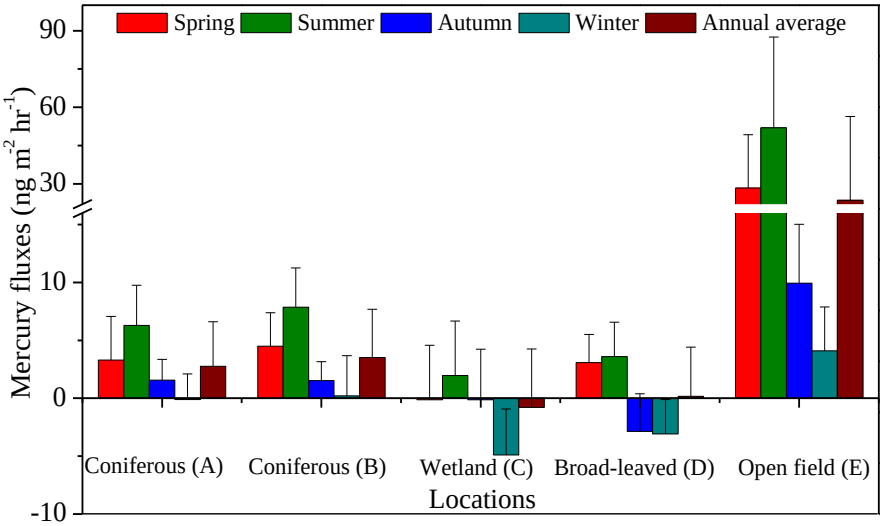

912

913 **Fig. 2.** Mean and standard deviation of soil-air TGM fluxes at the five plots for the four seasons and
914 annual values during the study. Plots A, B and C were located in the coniferous forest, plot D was
915 in the broad-leaved forest, and plot E was in the open field. The number of flux observations in
916 spring, summer, autumn and winter were 62, 92, 66 and 43, respectively.

917

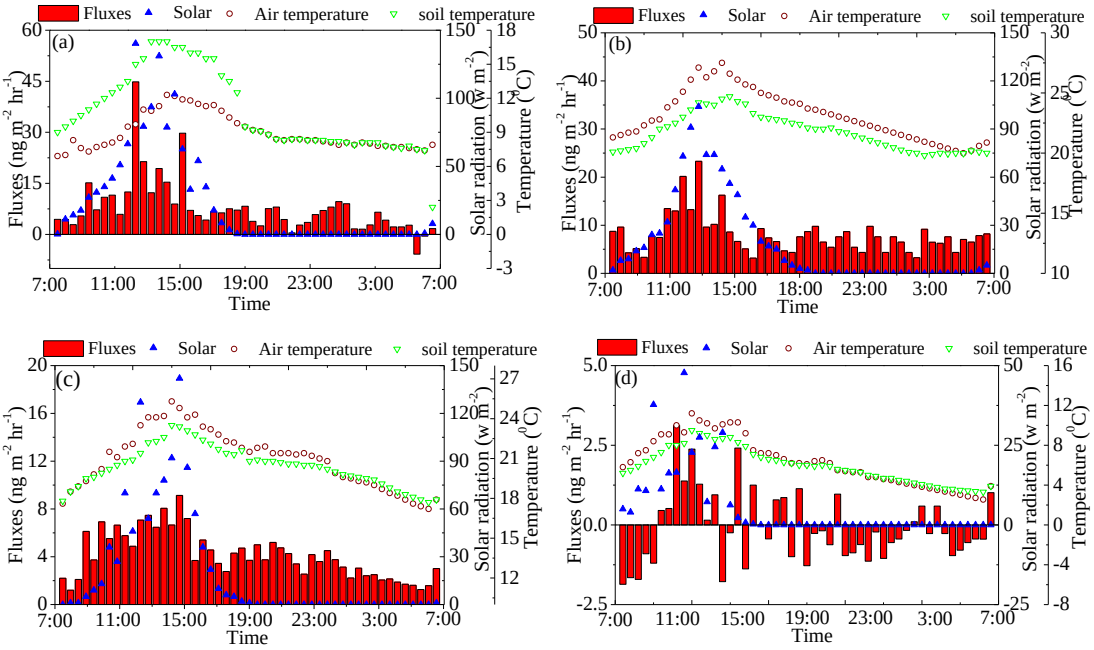

Fig. 3. The daily patterns of soil Hg fluxes with meteorological parameters in spring (a), summer (b), autumn (c) and winter (d) at the coniferous forest.

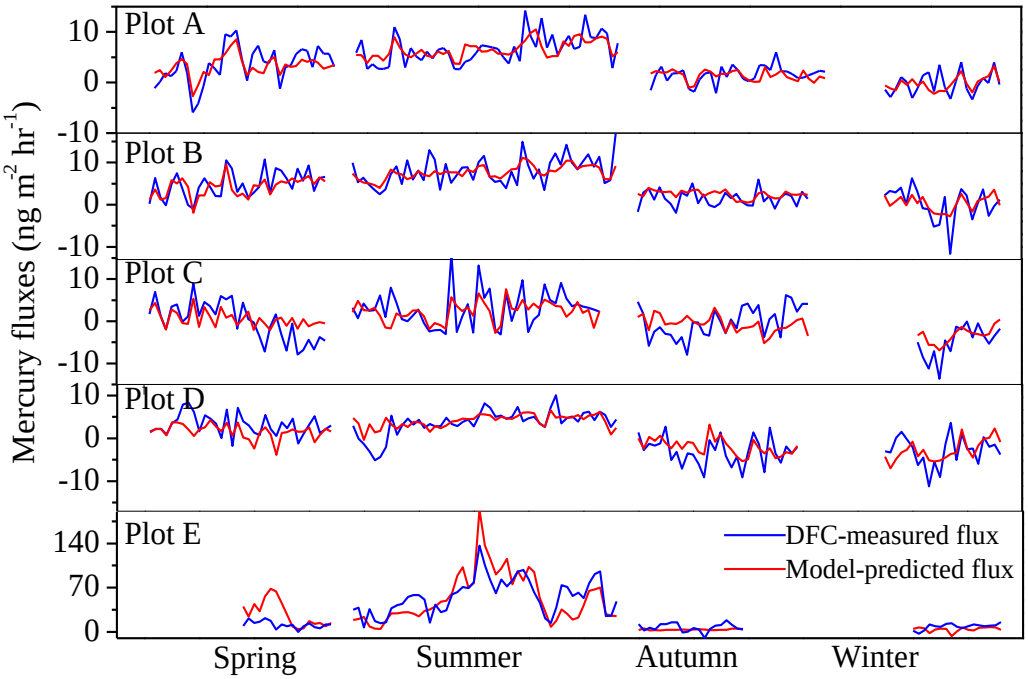

Fig. 4. Comparison between model-predicted and DFC-measured fluxes of Hg for the five plots. DFC-measured flux is a daily flux from averaged daytime and night values. Plot A was positioned on the top of the hill slope; plot B was in the middle of the hill slope; plot C was in the wetland within a coniferous forest; plot D was in broad-leaved (evergreen) forest and plot E is in open field.

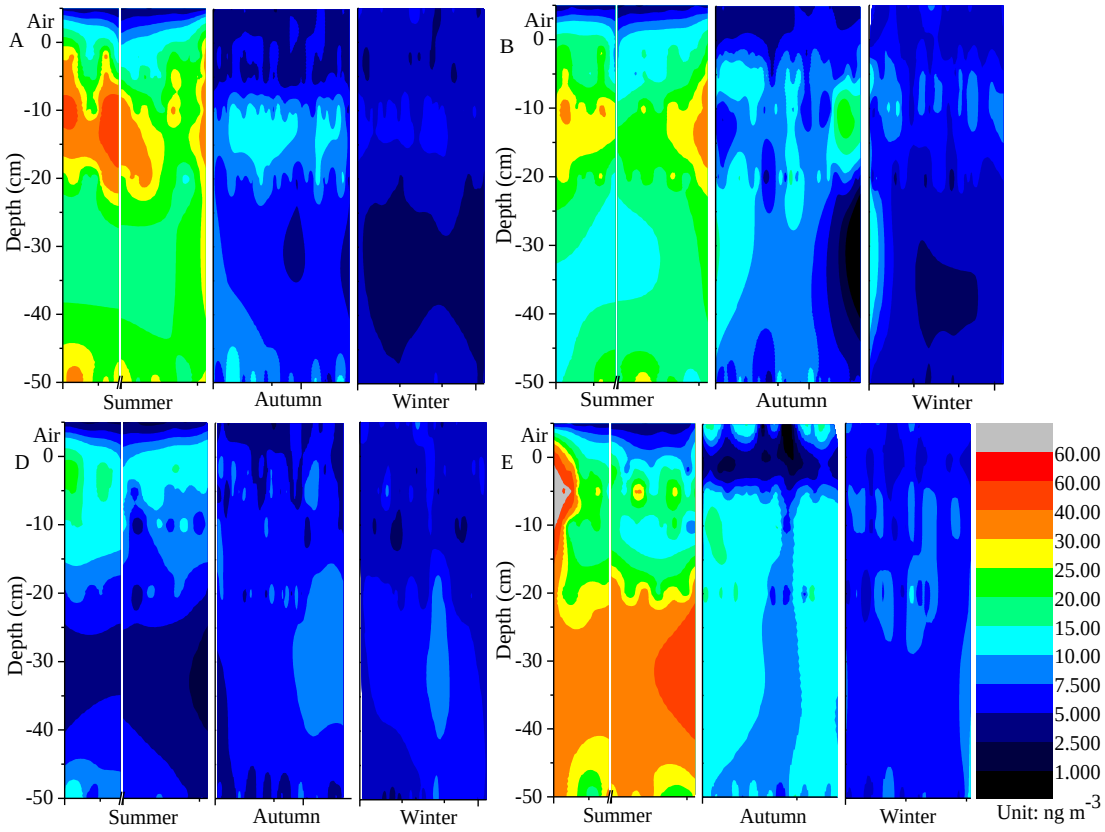

928

929

930 **Fig. 5.** Contour plots of soil pore TGM concentrations which in order are plots A, B, D and E. Plots
931 were created based on daytime and night pore TGM measurements combining soil surface (3 cm)
932 and 5 soil layers (3 cm, 6cm, 10cm, 20cm and 50cm).

933

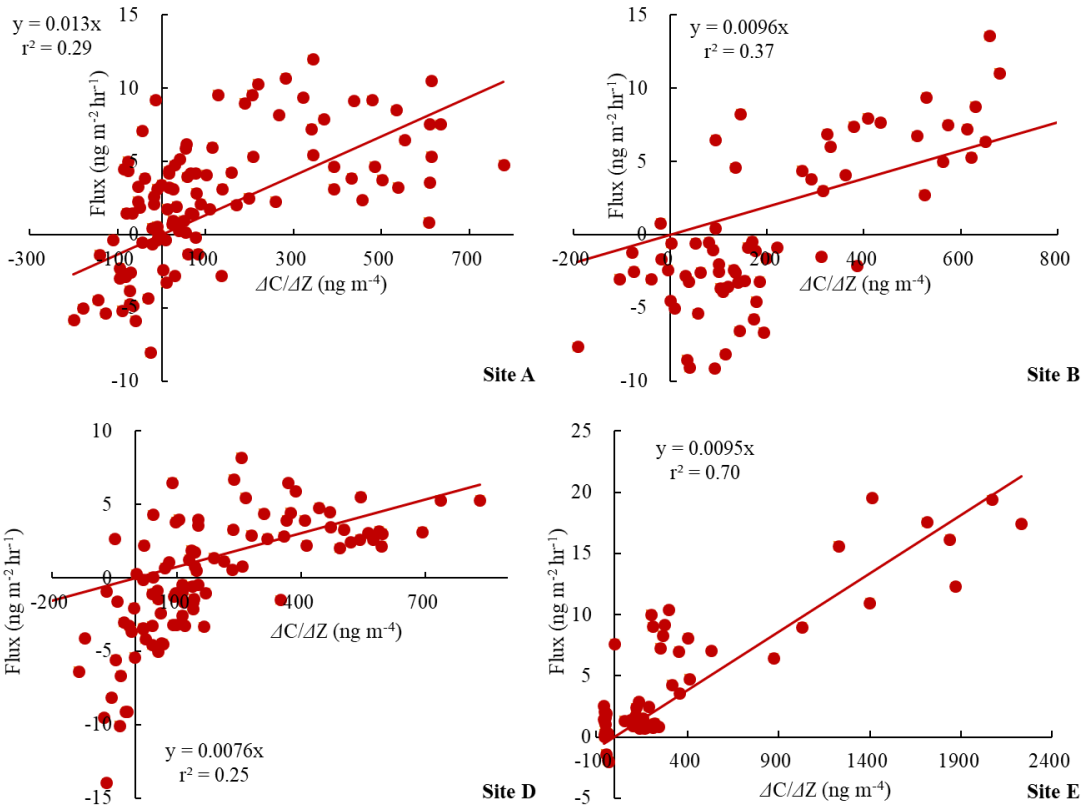

Fig. 6. Scatter plots and linear regressions between soil-air fluxes and the gradient of TGM concentration divided the distance between soil pore TGM at 3 cm (*Cs*) and the atmosphere above the plot (*Ca*) based on the two-resistance exchange interface model. The relationships were based on night flux and soil TGM measurements, and were significant at the respective plots ($p<0.05$).

Supporting Information

Soil emissions, soil air dynamics and model simulation of gaseous mercury in subtropical forest

Jun Zhou [a, b, c], Zhangwei Wang [a, b, *], Xiaoshan Zhang [a, b], Charles T. Driscoll [d], Che-Jen Lin [e]

a. Research Center for Eco-Environmental Sciences, Chinese Academy of Sciences, Beijing 100085, China

b. University of Chinese Academy of Sciences, Beijing 100049, China.

c. Key Laboratory of Soil Environment and Pollution Remediation, Institute of Soil Science, Chinese Academy of Sciences, Nanjing 210008, China

d. Department of Civil and Environmental Engineering, Syracuse University, 151 Link Hall, Syracuse, New York 13244, United States

e. Center for Advances in Water and Air Quality, Lamar University, Beaumont, Texas 77710, United States

* Corresponding author: Zhangwei Wang.

E-mail address: wangzhw@rcees.ac.cn(Z. Wang); Phone: +86 10 62849168.

No.18 Shuangqing Road, Beijing 100085, China

First author e-mail: zhoujun@issas.ac.cn (J. Zhou).

Contents:

19 Pages

4 Tables

10 Figures

Supporting Text:

Site description

The mean annual precipitation, temperature and daily relative humidity at the TFP are 1230 mm, 18.2 °C and 95%, respectively. The ecosystem type at the TFP study site is a Masson Pine dominated forest, with some associated ever-green broad-leaved species. Trees were planted in the 1960s. The soil is typically mountain yellow earth (corresponding to a Haplic Acrisol in FAO). The soil is acidic, with a pH of 3.79. From previous studies, the mean Hg concentrations in precipitation, throughfall, litterfall and organic soils were 55.3 ng L^{-1}, 98.9 ng L^{-1}, 104.8±18.6 ng g^{-1} and 191 ± 65 ng g^{-1}, respectively, with an annual Hg input of 291.2 μg m^{-2} yr^{-1}.(Zhou et al., 2016;Zhou et al., 2015)

Environmental measurements

Daily meteorological parameters were collected and averaged over 5-min intervals. Daily air temperature and solar radiation were monitored using a TP 101 digital thermometer and a GLZ−C photo synthetically radiometer (TOP Ltd. China), respectively, during diurnal measurements. Percent moisture was monitored with Time Domain Reflectometry (TDR) Hydra Probe II (SDI−12/RS485) and a Stevens water cable tester (USA). Measurements were taken at the same time with gold trap collection. Solar radiation was collected with a weather station (Davis Wireless Vantage VUE 06250 Weather Station, Davis Instruments, Hayward, CA) located in the TFP Forest Station about 500 m away from the sub-catchment.

For each DFC sampling location, bulk soil samples were collected from the DFC footprints (0−5 cm) in each month after the end of the measurement period. Soil samples were dried and homogenized, and completely ground to a fine powder in a pre-cleaned stainless-steel blender. The total Hg concentration in the soil samples was determined using a DMA-80 direct Hg analyzer (Milestone Ltd., Italy). SOM content in soils was determined using the sequential loss on ignition (LOI) method.(Zhou et al., 2013) A homogenized soil sample (WS) was dried at 105 °C for about 12- 24 h to obtain the dry weight of the samples (DW_{105}). The heated dry sample was then burned at 550 °C for 4 h and the weight of the sample after heating at 550 °C was DW_{550}. Thus, the TOM concentration (LOI_{550}) was calculated according to the following formula:

$$LOI_{550}=100(DW_{105}- DW_{550})/WS.$$

Statistical analysis

Mean pore TGM concentrations and soil TGM fluxes were compared among the five plots. Separate one-way ANOVAs were used to determine if the differences in Hg concentrations and fluxes were evident among the depths and plots. All differences in means were significant at the p=0.05 level and all means are reported with ± one standard deviation from the mean. The correlation was analyzed by Pearson's Correlation Tests using SPSS software (SPSS Inc. 16.0) and

correlation coefficient and p values are presented and significantly correlated at the level of 0.05.

Table S1. Characteristics and detail of measurements at five plots in the forested sub-catchments.

Plots	Locations	Date of flux measurement				Date of soil pore TGM measurement				SOM (0-5, %)	Area (%)
		Spring	Summer	Autumn	Winter	Spring	Summer	Autumn	Winter		
Plot A	Top of the hillslope of the coniferous forest	5 Mar-7 Apr	17 -19 Jun; 1-31 Jul; 10-24 Aug	3 Nov-6 Dec	24 Dec-14 Jan	5 Mar-7 Apr	17 -19 Jun; 21-31 Jul; 10-24 Aug	3 Nov-6 Dec	24 Dec-14 Jan	13.6	42.4
Plot B	Middle of the hill slope of the coniferous forest	5 Mar-7 Apr	17 -19 Jun; 1-31 Jul; 10-24 Aug	3 Nov-6 Dec	24 Dec-14 Jan		17 -19 Jun; 21-31 Jul; 10-24 Aug	3 Nov-6 Dec	24 Dec-14 Jan	16.3	42.4
Plot C	Wetland	5 Mar-7 Apr	1-31 Jul; 10-24 Aug	3 Nov-6 Dec	31 Dec-14 Jan					4.9	2.9
Plot D	Broad-leaved forest	5 Mar-7 Apr	17 -19 Jun; 1-31 Jul; 10-24 Aug	3 Nov-6 Dec	24 Dec-14 Jan	5 Mar-7 Apr	17 -19 Jun; 21-31 Jul; 10-24 Aug	3 Nov-6 Dec	24 Dec-14 Jan	8.8	10
Plot E	Open field (deserted agricultural land)	22 Mar-7 Apr	17 -19 Jun; 1-31 Jul; 10-24 Aug	3-23 Nov	30 Dec-14 Jan		17 -19 Jun; 21-31 Jul; 10-24 Aug	3-23 Nov	30 Dec-14 Jan	4.1	2.3

Table S2. A summary of empirical models in the literature for soil-air Hg fluxes.

Parameters	Soil type	Equations	References
Temperature	Forest lake and soil	F = EXP ($-E/RT$), E is the apparent activation energy; R is the gas constant.	(Xiao et al., 1991)
Temperature	Forest, open and agricultural fields.	Ln $F = E/RT + \beta_1$, E is the apparent activation energy; R is the gas constant.	(Carpi and Lindberg, 1997)
Temperature	Forest soil	Log $F = \beta_2 T + \beta_3$,	(Xu et al., 1999)
Temperature, soil Hg content	Bare soil	ln $F = -\gamma/T + \beta_4 \ln Sc + \beta_5$ γ is related to the apparent activation energy.	(Gbor et al., 2006)
Solar radiation, soil Hg content	Forest soil and artificially shaded background soil	ln $F = \beta_6 L + \beta_7 \ln Sc + \beta_8$	(Gbor et al., 2006)
Temperature, solar radiation	Forest soil during leaf-on period	$F = \beta_9 L + \beta_{10}$ EXP($\beta_{11} T$)	(Choi and Holsen, 2009)
Temperature	Forest soil during leaf-off period	$F = \beta_{12} + [\beta 1_3$ EXP($\beta_{14} T$ -1)]/β_{15}	(Choi and Holsen, 2009)
Temperature, solar radiation, soil moisture, Hg content	Laboratory study on background enriched Hg soil	$F = S_c \times [\beta_{16} + \beta_{17}$T + $\beta_{18} W + \beta_{19} L + \beta_{20} (T \times L) + \beta_{21} (T \times W) + \beta_{22} (W \times L) + \beta_{23} T^2 + \beta_{24} W^2 + \beta_{25} L^2]$	(Lin et al., 2010)
Temperature, solar radiation, Hg content	Bare soil and soil under the leaf canopy	$F = (10^{-3} \times S_c) \times [\beta_{26} + \beta_{27} T + \beta_{28} L + \beta_{29} (T \times L) + \beta_{30} T^2 + \beta_{31} L^2]$	(Kikuchi et al., 2013)
Temperature, solar radiation, soil moisture, Hg content, atmospheric TGM	Forest soil and bare soil	$F = (a \times S_c) \times [\partial_0 + \partial_1 T + \partial_2 W + \partial_3 L + \partial_4 C_a + \partial_5 (T \times W) + \partial_6 (T \times L) + \partial_7 (T \times C_a) + \partial_8 (W \times L) + \partial_9 (W \times Ca) + \partial_{10} (L \times C_a) + \partial_{11} T^2 + \partial_{12} W^2 + \partial_{13} L^2 + \partial_{14} C_a{}^2]$	This study

β_i is the coefficients of predictors in each equations and other parameters are same in the paper.

Table S3. Coefficients of the empirical models to predicting soil-air Hg fluxes using the annual data and corresponding environmental factors of the different ecosystems.

Coefficients	Coniferous forest	Wetland	Broad-leaved forest	Bare soil	Whole sub-catchment
∂_0	1.18	1.98	7.05×10^{-1}	1.13×10	1.39
∂_1	1.80×10^{-1}	1.39×10^{-1}	3.06×10^{-2}	−1.41	1.28×10^{-1}
∂_2	-1.13×10	−1.10	−9.24	4.48×10	−9.55
∂_3	1.05×10^{-2}	-2.37×10^{-2}	2.34×10^{-2}	2.75×10^{-3}	1.06×10^{-2}
∂_4	$-1..17\times10^{-1}$	−1.10	4.28×10^{-1}	-4.20×10^{-1}	-9.82×10^{-2}
∂_5	-1.27×10^{-1}	6.81×10^{-3}			-1.08×10^{-1}
∂_6	-2.43×10^{-4}	-1.13×10^{-4}	-5.11×10^{-4}	1.44×10^{-3}	-2.27×10^{-4}
∂_7					
∂_8				-4.91×10^{-2}	-1.13×10^{-3}
∂_9	-2.19×10^{-4}	2.55×10^{-1}	−2.61		-2.54×10^{-1}
∂_{10}				3.43×10^{-2}	7.90×10^{-7}
∂_{11}	-2.47×10^{-3}	-1.00×10^{-3}	4.19×10^{-4}	3.78×10^{-2}	-1.22×10^{-3}
∂_{12}	1.71×10		23.2×10	-1.05×10^{2}	1.44×10
∂_{13}	-4.88×10^{-5}	2.26×10^{-4}	-4.77×10^{-5}	-1.57×10^{-5}	-4.00×10^{-5}
∂_{14}		2.23×10^{-2}	3.33×10^{-2}		4.85×10^{-3}

Notes: Both first-order and second-order terms of the four factors investigated show net positive effects on the measured Hg fluxes within the data ranges of the regression analyses, and the corresponding equation is $F = (a \times S_c) \times [\partial_0 + \partial_1 T + \partial_2 W + \partial_3 L + \partial_4 C_a + \partial_5 (T\times W) + \partial_6 (T\times L) + \partial_7 (T\times C_a) + \partial_8 (W\times L) + \partial_9 (W\times Ca) + \partial_{10} (L\times C_a) + \partial_{11} T^2 + \partial_{12} W^2 + \partial_{13} L^2 + \partial_{14} C_a{}^2]$.

Table S4. Correlation coefficients of soil pore TGM concentrations in experimental plots with soil temperature, moisture and soil-air TGM fluxes for the four seasons and throughout the year.

Parameter	season	Plot A			Plot B			Plot D			Plot E		
		3	6	10	3	6	10	3	6	10	3	6	10
Soil temperature	Spr	0.37[a]	0.54[a]	0.48[a]				0.43[a]	0.09	0.13			
	Sum	0.43[a]	0.53[a]	0.40[a]	0.56[a]	0.32[b]	0.09	0.39[a]	0.42[a]	0.43[a]	0.42[a]	0.39[a]	0.34[b]
	Fall	0.46[a]	0.34[a]	0.08	0.56[a]	0.32[b]	0.09	0.32[b]	0.04	0.15	0.3[b]	0.3[b]	0.3[b]
	Win	0.25	0.45[a]	-0.01	0.34[b]	-0.06	0.34[b]	0.31[b]	0.16	0.09	0.43[b]	0.06	0
	Full year	0.85[a]	0.89[a]	0.83[a]	0.86[a]	0.74[a]	0.82[a]	0.84[a]	0.75[a]	0.67[a]	0.70[a]	0.67[a]	0.62[a]
Soil moisture	Spr	-0.18	-0.18	-0.02				-0.05	-0.05	-0.11			
	Sum	-0.22	-0.34[b]	-0.30[b]	-0.34[b]	-0.36[a]	-0.26	-0.32[b]	-0.27[b]	-0.40[a]	-0.1	-0.02	-0.16
	Fall	-0.03	0.09	-0.07	-0.34[b]	-0.36[a]	-0.26	0.03	-0.06	-0.01	-0.43[a]	-0.28	-0.28
	Win	-0.25	-0.24	0.25	0.16	0.13	0.22	-0.1	0.12	0.05	-0.28	-0.23	-0.38b
	Full year	-0.58[a]	-0.65[a]	-0.54[a]	-0.62[a]	-0.58[a]	-0.62[a]	-0.59[a]	-0.52[a]	-0.49[a]	-0.47[a]	-0.41[a]	-0.41[a]
Exchange fluxes	Spr	0.59[a]	0.41[a]	0.26[b]				0.49[a]	0.24	0.34[a]			
	Sum	0.42[a]	0.45[a]	0.36[a]	0.42[a]	0.26	0.18	0.51[a]	0.52[a]	0.27[b]	0.71[a]	0.59[a]	0.64[a]
	Fall	0.37[b]	0.35[a]	-0.12	0.42[a]	0.26	0.18	0.50[a]	0.12	0.09	0.33[b]	0.13	0.13
	Win	0.57[a]	0.53[a]	0.18	0.64[a]	-0.46[a]	0.25	0.51[a]	0.29	0.47[a]	0.65[a]	0.38[b]	0.3
	Full year	0.64[a]	0.65[a]	0.55[a]	0.72[a]	0.64[a]	0.67[a]	0.63[a]	0.51[a]	0.36[a]	0.77[a]	0.69[a]	0.65[a]

[a] Correlation is significant at the 0.01 level (two-tailed); [b] Correlation is significant at the 0.05 level (two-tailed). Note that soil temperature and moisture were directly determined in surface soil by Time Domain Reflectometry (TDR) with a Stevens water cable tester, not in each layer.

Figure Captions:

Fig. S1. The study area of the study area.(Wang et al., 2017)

Fig. S2. Correlation between the averaged solar radiation (8: 0-17:00) and daily soil-air Hg flux measured as the average of day and night values for the five plots.

Fig. S3. Effects of precipitation events on soil-air TGM fluxes at the five plots for the four seasons and annually.

Fig. S4. Correlation between the soil Hg concentrations ($S_c \pm SD$) and soil-air Hg flux ($F \pm SD$) under the forest canopy. Standard deviations of soil Hg concentrations were obtained from Hg concentrations in the four seasons (n=12). Because fluxes are often controlled by solar radiation for bare soils, the correlation analysis above does not include the open field (plot E).

Fig. S5. Correlation between the soil temperature and daily soil-air Hg flux measured as the average of day and night values for the five plots.

Fig. S6. Correlation between the soil moisture and daily soil-air Hg flux measured as the average of day and night values for the five plots.

Fig. S7. Correlation between the air TGM concentration and daily soil-air Hg flux measured as the average of day and night values for the five plots.

Fig. S8. Scatterplots of model-predicted and DFC-measured fluxes between soil and air in the Masson pine (a), wetland (b), camphor (c) and open field (d) plots.

Fig. S9. Hg (a) and TOM concentrations (b) with the soil depth at the collection depths of soil pore TGM.

Fig. S10. Correlation between the gradient of TGM concentrations between soil pore (3 cm) and atmosphere values and soil-air TGM flux at the four plots.

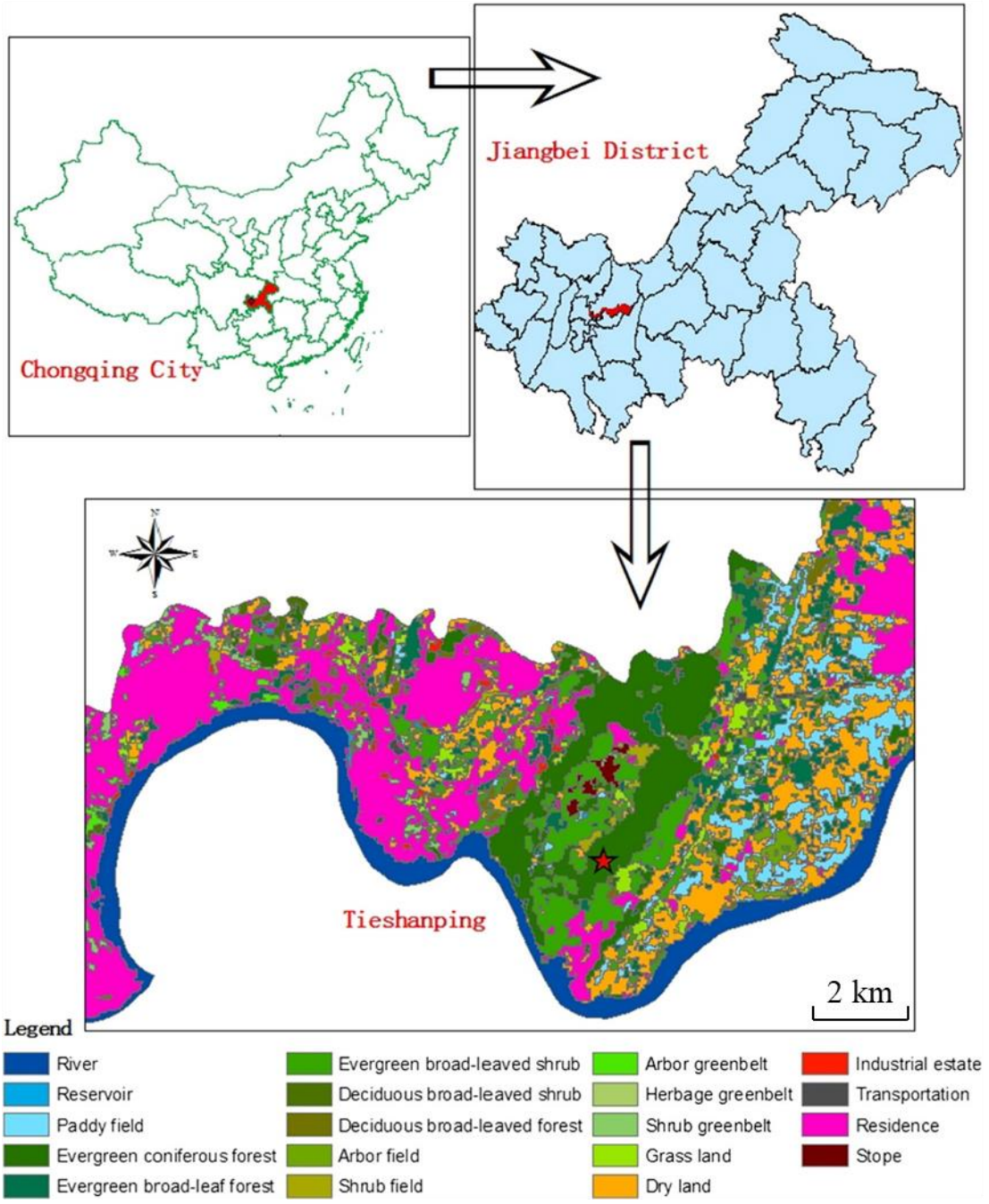

Fig. S1. The study area of a Masson pine dominated subtropical forest in Southwestern China. The total area of the studied forest was 1.06×10^3 ha and five plots representing the diverse ecosystems were selected at the sub-catchment (4.6 ha) (Wang et al., 2017).

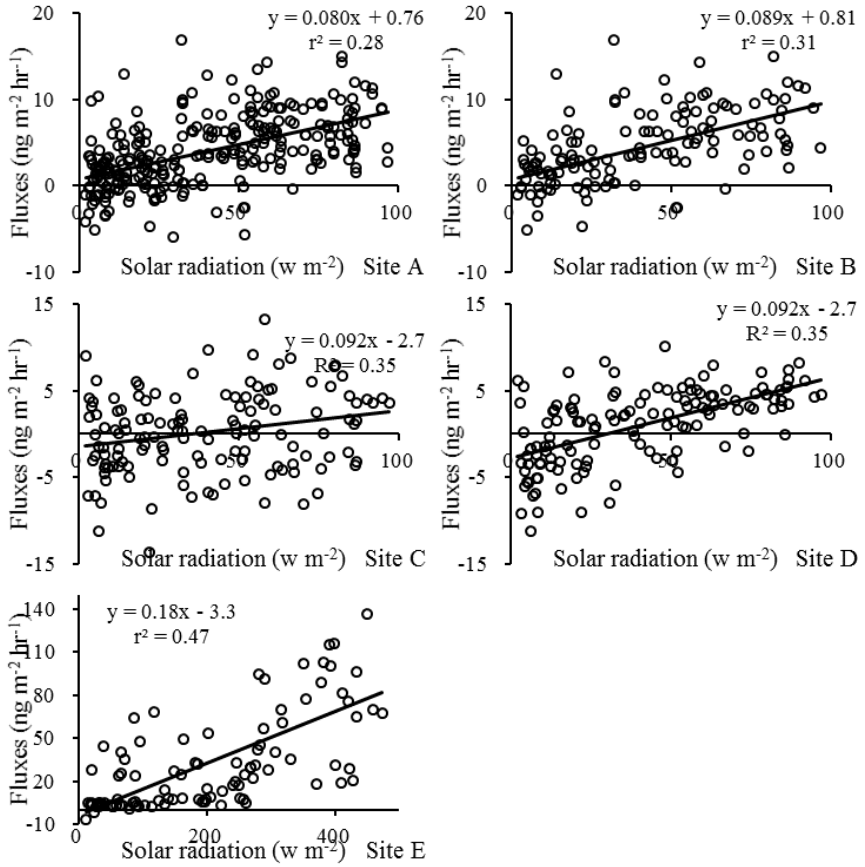

Fig. S2. Correlation between the averaged solar radiation (8: 0-17:00) and daily soil-air Hg flux measured as the average of day and night values for the five plots.

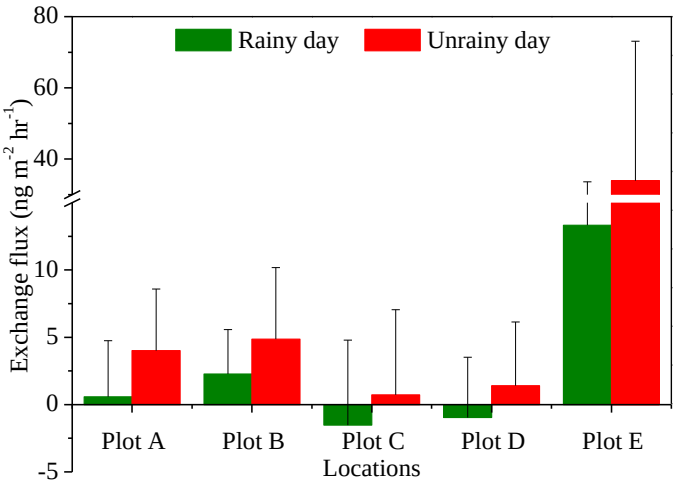

Fig. S3. Effects of precipitation events on soil-air TGM fluxes at the five plots for the four seasons and annually.

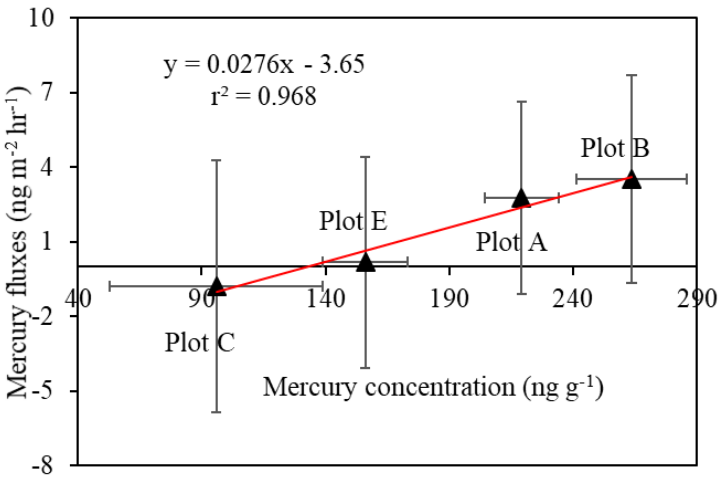

Fig. S4. Correlation between the soil Hg concentrations ($S_c \pm SD$) and soil-air Hg flux ($F \pm SD$) under the forest canopy. Standard deviations of soil Hg concentrations were obtained from Hg concentrations in the four seasons (n=12). Because fluxes are often controlled by solar radiation for bare soils, the correlation analysis above does not include the open field (plot E).

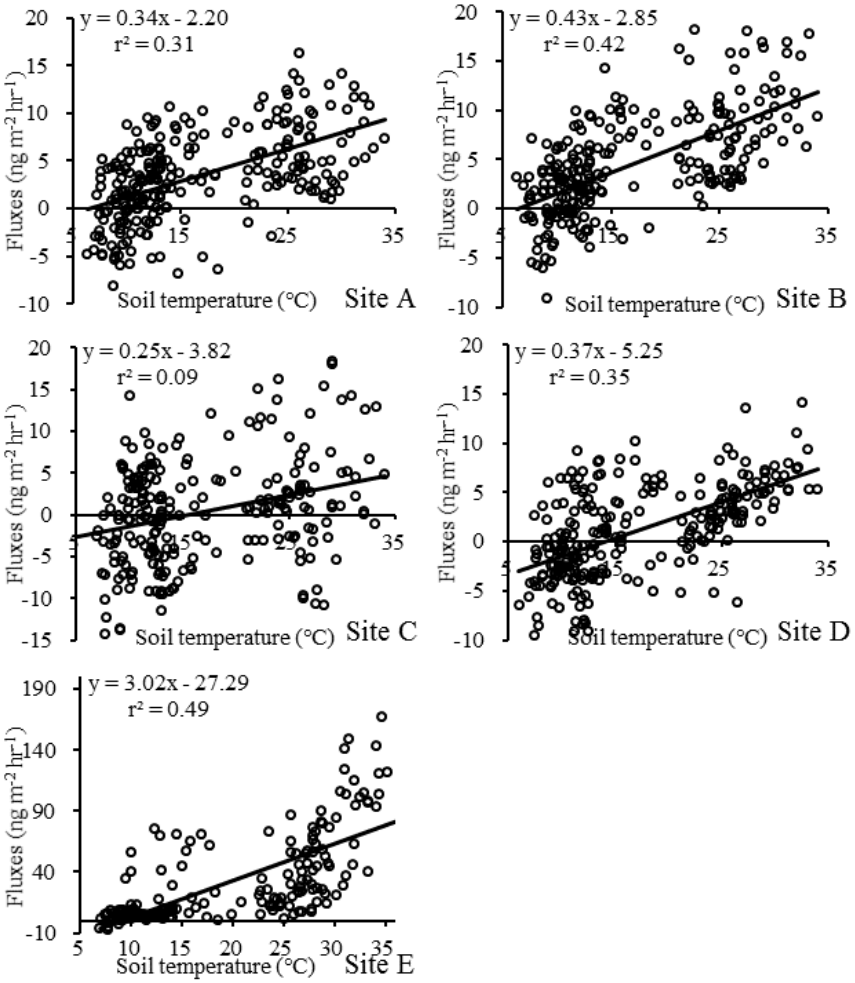

Fig. S5. Correlation between the soil temperature and daily soil-air Hg flux measured as the average of day and night values for the five plots.

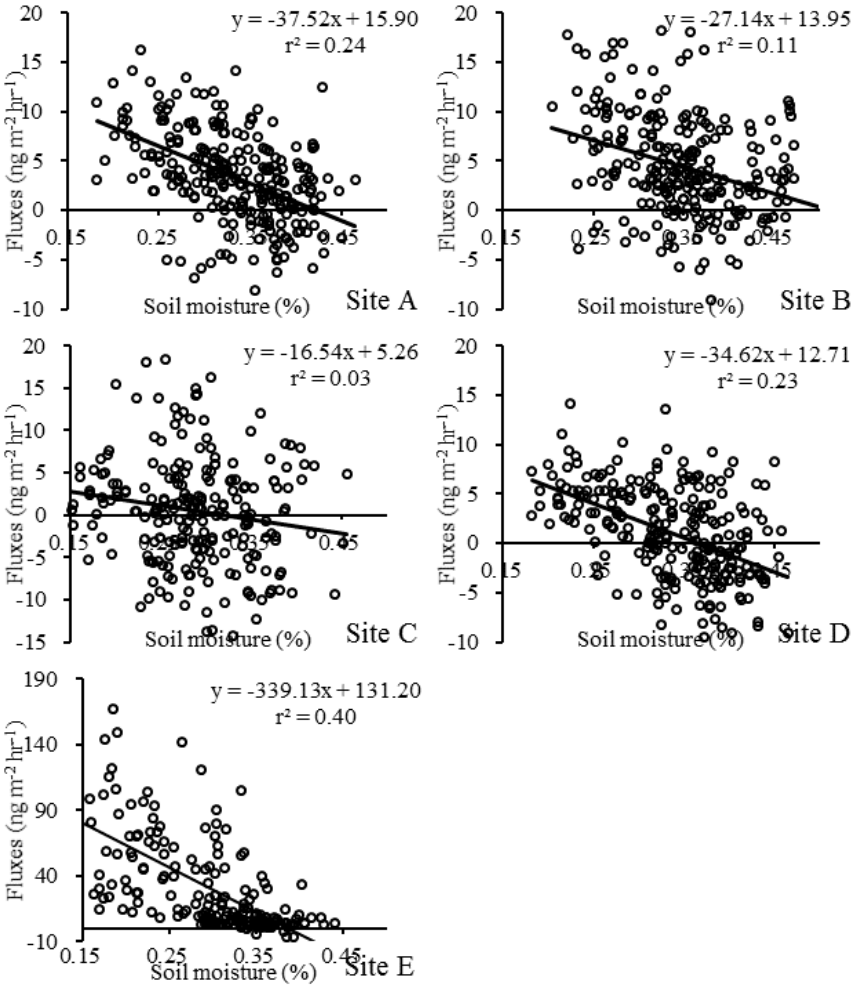

Fig. S6. Correlation between the soil moisture and daily soil-air Hg flux measured as the average of day and night values for the five plots.

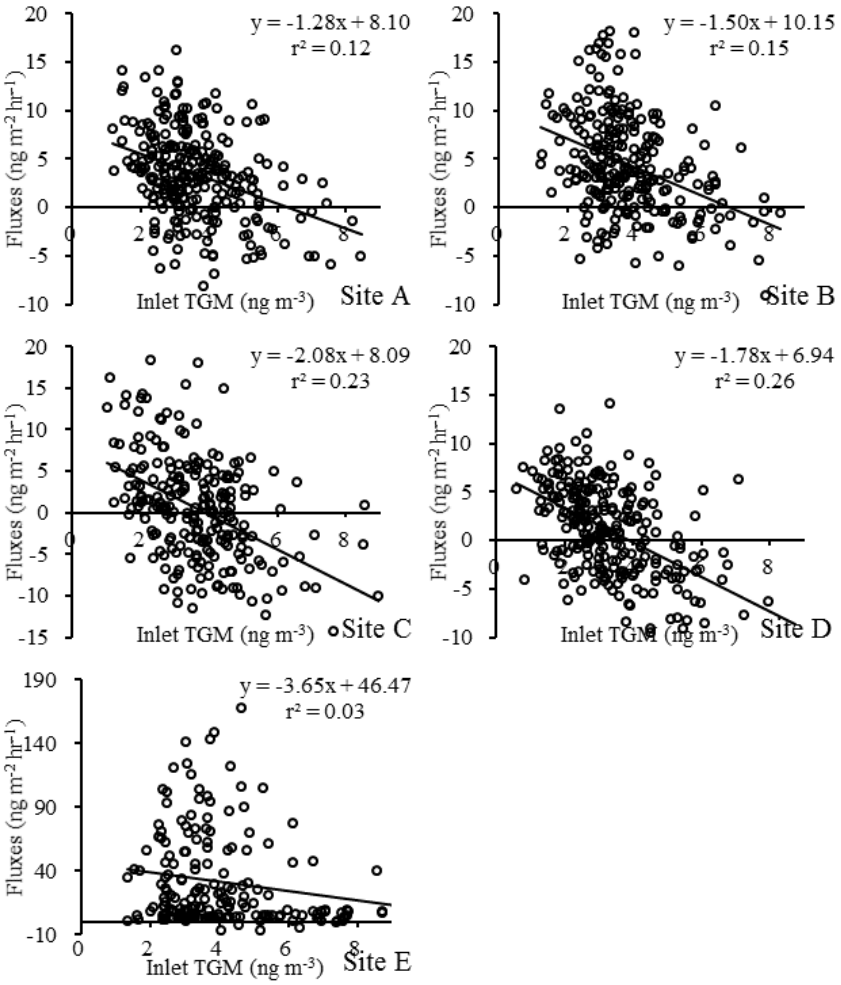

Fig. S7. Correlation between the air TGM concentration and daily soil-air Hg flux measured as the average of day and night values for the five plots.

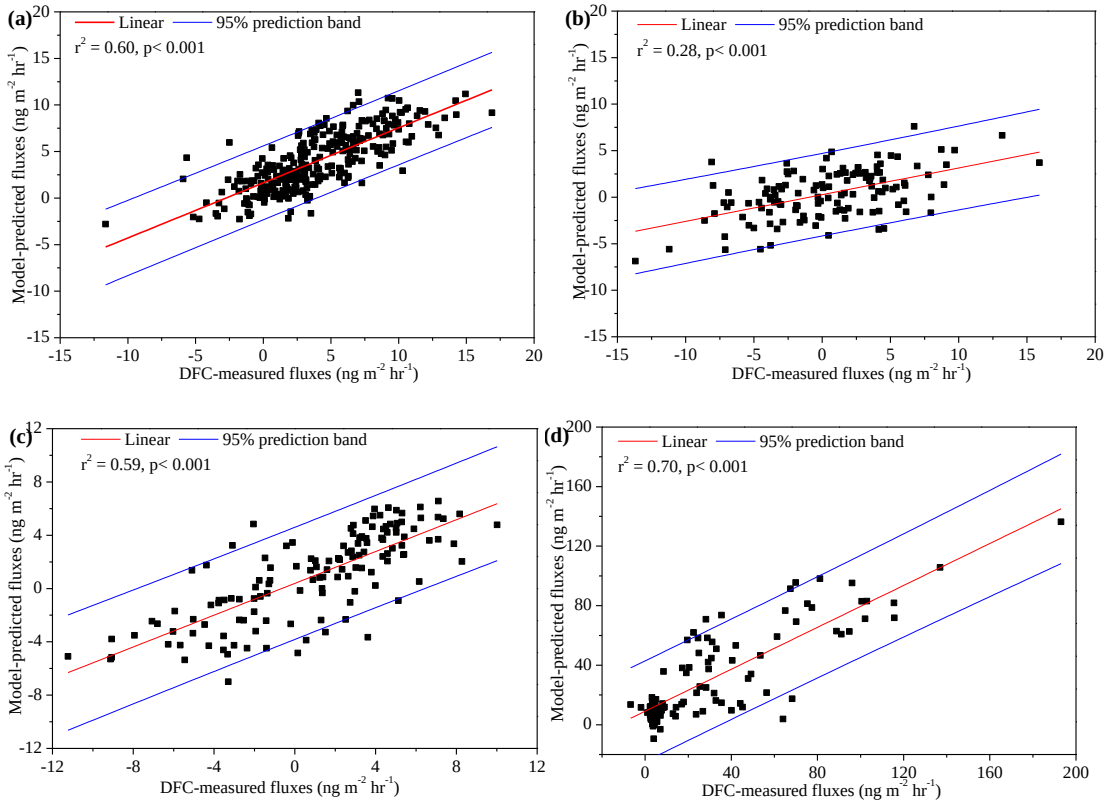

146

147

148 **Fig. S8.** Scatterplots of model-predicted and DFC-measured fluxes between soil and air in the
149 Masson pine (a), wetland (b), camphor (c) and open field (d) plots.

150

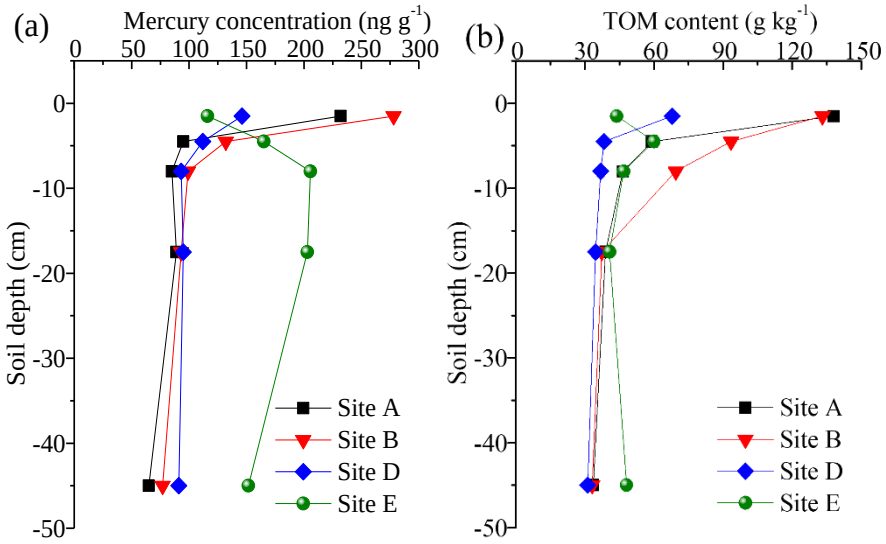

Fig. S9. Hg (a) and TOM concentrations (b) with the soil depth at the collection depths of soil pore TGM.

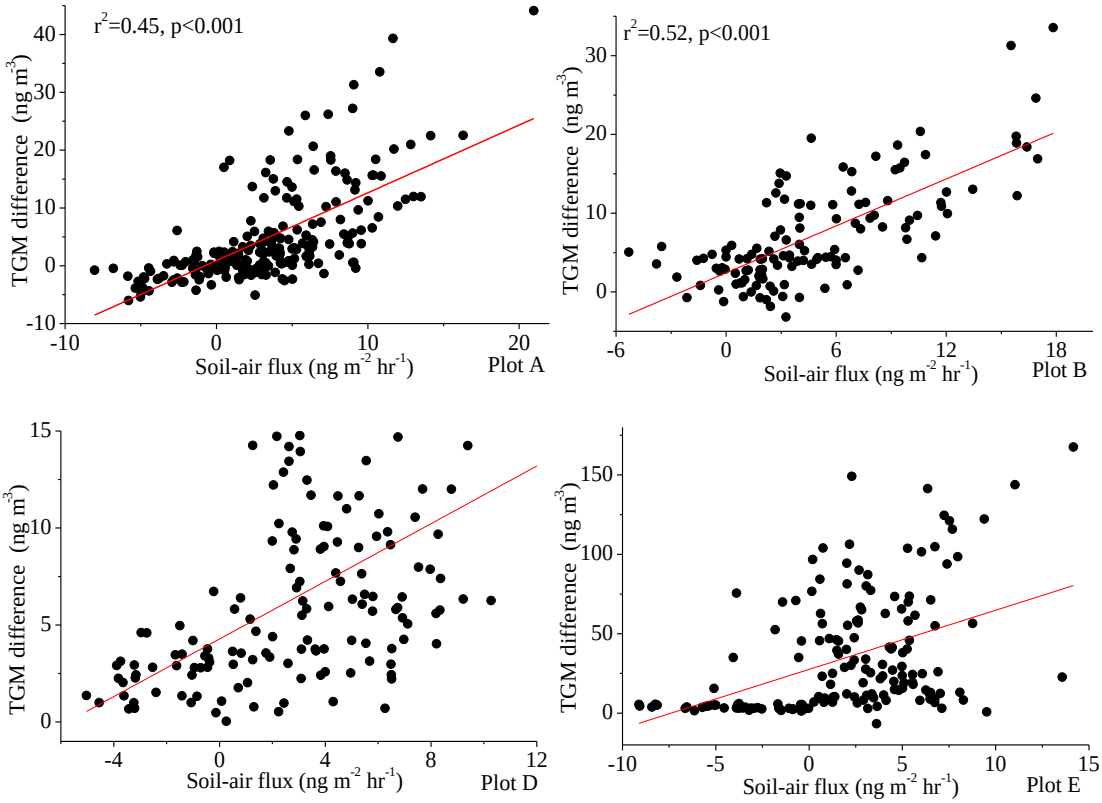

155

156

157 **Fig. S10.** Correlation between the gradient of TGM concentrations between soil pore (3 cm) and
158 atmosphere values and soil-air TGM flux at the four plots.

159

References:

Carpi, A., and Lindberg, S. E.: Sunlight-mediated emission of elemental mercury from soil amended with municipal sewage sludge, Environmental Science & Technology, 31, 2085-2091, 1997.

Choi, H.-D., and Holsen, T. M.: Gaseous mercury emissions from unsterilized and sterilized soils: The effect of temperature and UV radiation, Environmental pollution, 157, 1673-1678, 10.1016/j.envpol.2008.12.014, 2009.

Gbor, P. K., Wen, D., Meng, F., Yang, F., Zhang, B., and Sloan, J. J.: Improved model for mercury emission, transport and deposition, Atmospheric Environment, 40, 973-983, 2006.

Kikuchi, T., Ikemoto, H., Takahashi, K., Hasome, H., and Ueda, H.: Parameterizing soil emission and atmospheric oxidation-reduction in a model of the global biogeochemical cycle of mercury, Environmental Science & Technology, 47, 12266-12274, 2013.

Lin, C. J., Gustin, M. S., Singhasuk, P., Eckley, C., and Miller, M.: Empirical models for estimating mercury flux from soils, Environmental Science & Technology, 44, 8522-8528, 2010.

Wang, J., Zhang, X., Wang, Z., and Kang, R.: A relative method for measuring nitric oxide (NO) fluxes from forest soils, Science of the Total Environment, 574, 544-552, 10.1016/j.scitotenv.2016.09.012, 2017.

Xiao, Z. F., Munthe, J., Schroeder, W. H., and Lindqvist, O.: Vertical fluxes of volatile mercury over forest soil and lake surfaces in Sweden, Tellus Series B-Chemical and Physical Meteorology, 43, 267-279, 10.1034/j.1600-0889.1991.t01-1-00001.x, 1991.

Xu, X., Yang, X., Miller, D. R., Helble, J. J., and Carley, R. J.: Formulation of bi-directional atmosphere-surface exchanges of elemental mercury, Atmospheric Environment, 33, 4345-4355, 1999.

Zhou, J., Feng, X., Liu, H., Zhang, H., Fu, X., Bao, Z., Wang, X., and Zhang, Y.: Examination of total mercury inputs by precipitation and litterfall in a remote upland forest of Southwestern China, Atmospheric Environment, 81, 364-372, 10.1016/j.atmosenv.2013.09.010, 2013.

Zhou, J., Wang, Z., Zhang, X., and Chen, J.: Distribution and elevated soil pools of mercury in an acidic subtropical forest of southwestern China, Environmental pollution, 202, 187-195, 10.1016/j.envpol.2015.03.021, 2015.

Zhou, J., Wang, Z., Sun, T., Zhang, H., and Zhang, X.: Mercury in terrestrial forested systems with highly elevated mercury deposition in southwestern China: The risk to insects and potential release from wildfires, Environmental pollution, 212, 188-196, 10.1016/j.envpol.2016.01.003, 2016.